

Benchmark Suggestions for Resonant Double Higgs Production at the LHC for Extended Higgs Sectors

Sebastian Baum,^{a,b} Nausheen R. Shah^c

^a*The Oskar Klein Centre for Cosmoparticle Physics, Department of Physics, Stockholm University, Alba Nova, 10691 Stockholm, Sweden*

^b*Nordita, KTH Royal Institute of Technology and Stockholm University, Roslagstullsbacken 23, 10691 Stockholm, Sweden*

^c*Department of Physics & Astronomy, Wayne State University, Detroit, MI 48201, USA*

E-mail: sbaum@fysik.su.se, nausheen.shah@wayne.edu

ABSTRACT: In this note we present benchmark scenarios for resonant double Higgs production at the 13 TeV LHC in the 2HDM+S model and the Z_3 Next-to-Minimal Supersymmetric Standard Model (NMSSM), which may be accessible with 300 fb^{-1} of data. The NMSSM Higgs sector can be mapped onto the 2HDM+S. We show benchmark points and relevant parameter planes in the 2HDM+S for three sets of signatures: $(A \rightarrow h_{125}a, H \rightarrow h_{125}h)$, $(A \rightarrow ah, H \rightarrow hh, H \rightarrow aa)$, and $(H \rightarrow h_{125}h_{125})$. The first two signatures are optimized in what we call *Z-Phobic* scenarios where H/A decays into final states with Z bosons are suppressed. The last signature, h_{125} pair production, is directly proportional to the misalignment of h_{125} with the interaction states sharing the couplings of a SM Higgs boson, and hence is presented in the *Max Misalignment* scenario. We also present two NMSSM benchmark points for the $(A \rightarrow h_{125}a, H \rightarrow h_{125}h)$ signatures. The benchmark scenarios presented here are based on Refs. [1, 2].

Contents

1	Introduction	1
2	The 2HDM+S	1
2.1	Z-Phobic Scenarios:	7
2.1.1	Z-Phobic: $h_{125}+\text{Visible}$ ($H \rightarrow h_{125}a$ and $A \rightarrow h_{125}h$)	8
2.1.2	Z-Phobic: $h_{125}+\text{Invisible}$ ($H \rightarrow h_{125}a$ and $A \rightarrow h_{125}h$)	15
2.1.3	Z-Phobic: Double Singlet Scenario ($H \rightarrow hh$, $H \rightarrow aa$, and $A \rightarrow ha$)	18
2.2	Max Misalignment Scenario: $H \rightarrow h_{125}h_{125}$	20
3	NMSSM Benchmarks	26
4	Conclusions	31

1 Introduction

In this note we present benchmark scenarios for resonant double Higgs production at the 13 TeV LHC in the 2HDM+S and the Next-to-Minimal Supersymmetric Standard Model (NMSSM). We refer the reader to Ref. [1] for a detailed description of the 2HDM+S, in Sec. 2 we give only a brief summary of the most important aspects of the 2HDM+S before presenting benchmark scenarios for resonant double Higgs production. Some recent work on resonant pair production of SM-like Higgs bosons in 2HDMs and the pMSSM can also be found in Refs. [3, 4].

In Sec. 3 we present benchmark scenarios for double Higgs production in the Z_3 NMSSM, previously published in Ref. [2]. The 2HDM+S constitutes a generalized version of the NMSSM's Higgs sector, see Ref. [1] for a mapping of both the general and the Z_3 NMSSM to the 2HDM+S. Additional benchmark scenarios for double Higgs production in the NMSSM have e.g. been published in Ref. [5].

2 The 2HDM+S

We consider an extension of the Standard Model (SM) with a Higgs sector comprised of two $SU(2)$ -doublets and a complex gauge singlet scalar, dubbed the 2HDM+S. Such an extended Higgs sector is of high interest since it constitutes a generalized version of the Next-to-Minimal Supersymmetric Standard Model's (NMSSM's) Higgs Sector. For a detailed description of the 2HDM+S, its phenomenology, and the mapping to both the general and the Z_3 NMSSM, see Ref. [1]. We will only reproduce the portion of the analysis from Refs. [1, 2] relevant for the description of the benchmark scenarios presented here.

We will assume a type-II Yukawa structure for the coupling of the Higgs bosons to SM fermions, as is expected in generic supersymmetric theories. Note that for the purposes

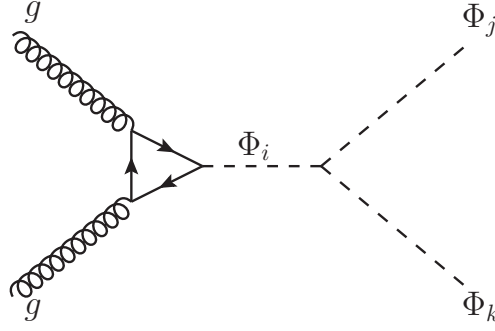


Figure 1: Illustration of resonant double Higgs production in the 2HDM+S. The Φ_i stand for any of the neutral Higgs bosons. Note that CP conservation requires either all three states to be CP-even (e.g. $H \rightarrow h_{125}h$) or two of the states to be CP-odd and the third to be CP-even (e.g. $A \rightarrow h_{125}a$).

of this note, we consider the low $\tan \beta$ regime (in particular, we present benchmarks for fixed $\tan \beta = 2.5$), where a different choice for the Yukawa structure would yield similar numerical results.

The scalar sector of the 2HDM+S is comprised of 6 physical states,

$$\{h_{125}, h, H\}, \quad \{a, A\}, \quad H^\pm. \quad (2.1)$$

The first three are the neutral CP-even states, a and A are the two CP-odd neutral states, and H^\pm is the charged Higgs. Of the CP-even states, h_{125} is identified with the SM-like 125 GeV state observed at the LHC, and the remaining states are order by their masses, $m_h < m_H$. Likewise, $m_a < m_A$.

It is useful to write the neutral Higgs states in terms of the interaction states of the extended Higgs basis [6–13]

$$h_i = S_{h_i}^{\text{SM}} H^{\text{SM}} + S_{h_i}^{\text{NSM}} + S_{h_i}^{\text{S}}, \quad (2.2)$$

for the CP-even states $h_i = \{h_{125}, h, H\}$, and

$$a_i = P_{a_i}^{\text{NSM}} A^{\text{NSM}} + P_{a_i}^{\text{S}} A^{\text{S}}, \quad (2.3)$$

for the CP-odd states $a_i = \{a, A\}$. In a type-II Yukawa structure, the coupling of the Higgs basis eigenstates to pairs of SM particles can be written as

$$H^{\text{SM}}(\text{up}, \text{down}, \text{VV}) = (g_{\text{SM}}, g_{\text{SM}}, g_{\text{SM}}), \quad (2.4)$$

$$H^{\text{NSM}}(\text{up}, \text{down}, \text{VV}) = (-g_{\text{SM}}/\tan \beta, g_{\text{SM}} \tan \beta, 0), \quad (2.5)$$

$$H^{\text{S}}(\text{up}, \text{down}, \text{VV}) = (0, 0, 0), \quad (2.6)$$

$$A^{\text{NSM}}(\text{up}, \text{down}, \text{VV}) = (g_{\text{SM}}/\tan \beta, g_{\text{SM}} \tan \beta, 0), \quad (2.7)$$

$$A^{\text{S}}(\text{up}, \text{down}, \text{VV}) = (0, 0, 0), \quad (2.8)$$

where “up” (“down”) stands for pairs of up-type (down-type) SM fermions, “VV” for pairs of massive vector bosons, and g_{SM} is the coupling of a SM Higgs boson to such particles.

The parameter space of the 2HDM+S can be intuitively described in terms of the physical masses

$$m_{h_{125}} , \quad m_H , \quad m_h , \quad m_A , \quad m_a , \quad m_{H^\pm} , \quad (2.9)$$

the mixing angles

$$S_{h_{125}}^{\text{NSM}} , \quad S_{h_{125}}^{\text{S}} , \quad S_H^{\text{S}} , \quad P_A^{\text{S}} , \quad (2.10)$$

the vacuum expectation values (vevs) of the 2 doublets and the singlet, which we parameterize by

$$v , \quad \tan \beta , \quad v_S , \quad (2.11)$$

10 independent trilinear couplings between the interaction states of the extended Higgs basis

$$\begin{aligned} & \{g_{H^{\text{SM}} H^{\text{NSM}} H^{\text{NSM}}}, \quad g_{H^{\text{SM}} H^{\text{S}} H^{\text{S}}}, \quad g_{H^{\text{SM}} A^{\text{S}} A^{\text{S}}}\}, \\ & \{g_{H^{\text{NSM}} H^{\text{NSM}} H^{\text{NSM}}}, \quad g_{H^{\text{NSM}} H^{\text{NSM}} H^{\text{S}}}, \quad g_{H^{\text{NSM}} H^{\text{S}} H^{\text{S}}}, \quad g_{H^{\text{NSM}} A^{\text{S}} A^{\text{S}}}\}, \\ & \{g_{H^{\text{S}} H^{\text{S}} H^{\text{S}}}, \quad g_{H^{\text{S}} A^{\text{NSM}} A^{\text{S}}}, \quad g_{H^{\text{S}} A^{\text{S}} A^{\text{S}}}\} . \end{aligned} \quad (2.12)$$

and 4 independent quartic couplings

$$\{\lambda_{H^{\text{NSM}} H^{\text{NSM}} H^{\text{S}} H^{\text{S}}}, \quad \lambda_{H^{\text{NSM}} H^{\text{NSM}} A^{\text{S}} A^{\text{S}}}, \quad \lambda_{H^{\text{S}} H^{\text{S}} A^{\text{S}} A^{\text{S}}}, \quad \lambda_{A^{\text{S}} A^{\text{S}} A^{\text{S}} A^{\text{S}}}\}. \quad (2.13)$$

All couplings, in particular the remaining trilinear couplings which play an important role for resonant double Higgs production, are fixed in terms of the above parameters.

Let us comment on the sign conventions we use for the mixing angles. The conventions are particularly relevant when reconstructing the full mixing matrix of the CP-even states from our input parameters $\{S_{h_{125}}^{\text{NSM}}, S_{h_{125}}^{\text{S}}, S_H^{\text{S}}\}$. Assuming no CP violation, the mixing matrix can be written as

$$\begin{pmatrix} h_{125} \\ H \\ h \end{pmatrix} = \begin{pmatrix} c_{12}c_{13} & s_{12}c_{13} & s_{13} \\ -s_{12}c_{23} - c_{12}s_{23}s_{13} & c_{12}c_{23} - s_{12}s_{23}s_{13} & s_{23}c_{13} \\ s_{12}s_{23} - c_{12}c_{23}s_{13} & -c_{12}s_{23} - s_{12}c_{23}s_{13} & c_{23}c_{13} \end{pmatrix} \begin{pmatrix} H^{\text{SM}} \\ H^{\text{NSM}} \\ H^{\text{S}} \end{pmatrix}, \quad (2.14)$$

where $s_{12} \equiv \sin \theta_{12}$, etc. In order to obtain all of the entries of the mixing matrix, we use the following identifications:

- $s_{13} = S_{h_{125}}^{\text{S}}$,
- $c_{13} = \sqrt{1 - s_{13}^2}$,
- $s_{12} = S_{h_{125}}^{\text{NSM}}/c_{13}$,
- $c_{12} = \sqrt{1 - s_{12}^2}$,
- $s_{23} = S_H^{\text{S}}/c_{13}$,
- $c_{23} = \sqrt{1 - s_{23}^2}$.

Thus, we choose $\text{sgn}(c_{ij}) \geq 0$ everywhere. However, since the s_{ij} can take both signs (depending on the signs of the inputs $\{S_{h_{125}}^{\text{NSM}}, S_{h_{125}}^{\text{S}}, S_H^{\text{S}}\}$), we can explore all possible configurations of the mixing angles by varying the signs of the input values.

The SM-like nature of the observed 125 GeV state is achieved in the 2HDM+S by enforcing approximate alignment

$$\{(S_{h_{125}}^{\text{NSM}})^2, (S_{h_{125}}^{\text{S}})^2\} \ll 1, \quad (2.15)$$

and fixing $m_{h_{125}} \approx 125$ GeV. Of particular interest for LHC phenomenology is the alignment-without-decoupling limit, where A and H remain relatively light. Then, the structure of the potential enforces the couplings between pairs of SM-like states and a non SM-like Higgs, $g_{h_{125}h_{125}H}$, to vanish, since in this limit [1]

$$\{g_{H^{\text{SM}}H^{\text{SM}}H^{\text{NSM}}}, g_{H^{\text{SM}}H^{\text{SM}}H^{\text{S}}}\} \rightarrow 0 \quad (2.16)$$

For the purposes of this note, we are interested in resonant double Higgs production channels such as $(gg \rightarrow \Phi_i \rightarrow \Phi_j + \Phi_k)$, cf. Fig. 1, where the Φ_i stand for any of the neutral Higgs bosons. Thus, we consider the charged Higgs to be sufficiently heavy such that it will not affect the decays of the neutral states, e.g. $m_{H^\pm} > 1$ TeV. Further, we note that $(\Phi_i \rightarrow Z\Phi_j)$ decays give rise to search channels for the 2HDM+S complimentary to $(\Phi_i \rightarrow \Phi_j + \Phi_k)$ channels, cf. Ref. [1]. CP-conservation allows decays into pairs of Higgs bosons only if they are of the type $(h_i \rightarrow h_j h_k)$, $(h_i \rightarrow a_j a_k)$, or $(a_i \rightarrow h_j a_k)$, while decays into a Z and a Higgs boson must be of the type $(h_i \rightarrow Z a_j)$ or $(a_i \rightarrow Z h_j)$. Further, decays into pairs of either Z or W gauge bosons are only allowed for the CP-even states, $(h_i \rightarrow ZZ/W^+W^-)$. The corresponding partial widths are given by

$$\Gamma(\Phi_i \rightarrow \Phi_j \Phi_k) = \frac{g_{\Phi_i \Phi_j \Phi_k}^2}{16\pi m_{\Phi_i}} \left(\frac{1}{1 + \delta_{jk}} \right) \sqrt{1 - 2 \frac{m_{\Phi_j}^2 + m_{\Phi_k}^2}{m_{\Phi_i}^2} + \frac{(m_{\Phi_j}^2 - m_{\Phi_k}^2)^2}{m_{\Phi_i}^4}}, \quad (2.17)$$

$$\begin{aligned} \Gamma(\Phi_i \rightarrow Z\Phi_j) &= \frac{(C_{\Phi_i}^{\text{NSM}} C_{\Phi_j}^{\text{NSM}})^2}{32\pi} \frac{m_Z^2}{m_{\Phi_i} v^2} \left[\frac{(m_{\Phi_i}^2 - m_{\Phi_j}^2)^2}{m_Z^2} - 2(m_{\Phi_i}^2 + m_{\Phi_j}^2) + m_Z^2 \right] \\ &\quad \times \sqrt{1 - 2 \frac{m_{\Phi_j}^2 + m_Z^2}{m_{\Phi_i}^2} + \frac{(m_{\Phi_j}^2 - m_Z^2)^2}{m_{\Phi_i}^4}}, \end{aligned} \quad (2.18)$$

$$\Gamma(h_i \rightarrow ZZ) = \frac{(S_{h_i}^{\text{SM}})^2 m_Z^4}{16\pi m_{h_i} v^2} \left(3 - \frac{m_{h_i}^2}{m_Z^2} + \frac{m_{h_i}^4}{4m_Z^4} \right) \sqrt{1 - 4 \frac{m_Z^2}{m_{h_i}^2}}, \quad (2.19)$$

$$\Gamma(h_i \rightarrow W^+W^-) = \frac{(S_{h_i}^{\text{SM}})^2 m_W^4}{8\pi m_{h_i} v^2} \left(3 - \frac{m_{h_i}^2}{m_W^2} + \frac{m_{h_i}^4}{4m_W^4} \right) \sqrt{1 - 4 \frac{m_W^2}{m_{h_i}^2}}, \quad (2.20)$$

where we use C_Φ^J to refer to the mixing angles for both the CP-even and the CP-odd mass eigenstates Φ with mass m_Φ ; for example, $C_\Phi^{\text{NSM}} = S_{h_i}^{\text{NSM}}$ or $P_{a_i}^{\text{NSM}}$ depending on context.

For partial widths into pairs of SM fermions, see Ref. [1]. The trilinear couplings between the Higgs mass eigenstates are given by

$$\begin{aligned} g_{h_i h_j h_k} &= \sum_{H^l} \sum_{H^m} \sum_{H^n} S_{h_i}^{H^l} S_{h_j}^{H^m} S_{h_k}^{H^n} g_{H^l H^m H^n} , \\ g_{h_i a_j a_k} &= \sum_{H^l} \sum_{A^m} \sum_{A^n} S_{h_i}^{H^l} P_{a_j}^{A^m} P_{a_k}^{A^n} g_{H^l A^m A^n} , \end{aligned} \quad (2.21)$$

where the $g_{H^l H^m H^n}$ and $g_{H^l A^m A^n}$ are the couplings between the interaction states of the Higgs basis. The exact expressions for these trilinear couplings can be found in App. B of Ref. [1]. Note that all trilinear couplings involving at least a pair of H^{SM} states, e.g. $g_{H^{\text{SM}} H^{\text{SM}} H^{\text{NSM}}}$, as well as the couplings $g_{H^{\text{SM}} H^{\text{NSM}} H^{\text{S}}}$ and $g_{H^{\text{SM}} A^{\text{NSM}} H^{\text{S}}}$ are proportional to the entries of the scalar mass matrices, which are in turn determined by the physical masses and the mixing angles. The scale of most of the remaining couplings, in particular the couplings $g_{H^{\text{NSM}} H^{\text{S}} H^{\text{S}}}$, $g_{H^{\text{NSM}} A^{\text{S}} A^{\text{S}}}$, and $g_{H^{\text{S}} A^{\text{NSM}} A^{\text{S}}}$, which will become important in Sec. 2.1.3, is set by v .

In the limit of perfect alignment, the relevant couplings for decays into one SM-like and one non SM-like state, i.e. ($H \rightarrow h_{125} h$) and ($A \rightarrow h_{125} a$), can be written as

$$g_{h_{125} H h} = \frac{S_H^{\text{NSM}} S_H^{\text{S}}}{\sqrt{2}v} \left\{ [1 - 2(S_H^{\text{S}})^2] (m_H^2 - m_h^2) + \sqrt{2}v \tilde{g}_H \right\} , \quad (2.22)$$

$$g_{h_{125} A a} = \frac{P_A^{\text{NSM}} P_A^{\text{S}}}{\sqrt{2}v} \left\{ [1 - 2(P_A^{\text{S}})^2] (m_A^2 - m_a^2) + \sqrt{2}v \tilde{g}_A \right\} , \quad (2.23)$$

where we have defined

$$\tilde{g}_H \equiv (g_{H^{\text{SM}} H^{\text{S}} H^{\text{S}}} - g_{H^{\text{SM}} H^{\text{NSM}} H^{\text{NSM}}}) , \quad (2.24)$$

$$\tilde{g}_A \equiv (g_{H^{\text{SM}} A^{\text{S}} A^{\text{S}}} - g_{H^{\text{SM}} A^{\text{NSM}} A^{\text{NSM}}}) . \quad (2.25)$$

The scale of the trilinear couplings entering \tilde{g}_H and \tilde{g}_A is set by v . Since ($H \rightarrow h_{125} h$) and ($A \rightarrow h_{125} a$) decays require sizable mass splittings between H and h or A and a , respectively, we expect the contribution of the \tilde{g}_H to $g_{h_{125} H h}$ and \tilde{g}_A to $g_{h_{125} A a}$ to be sub-dominant, unless $(S_H^{\text{S}})^2 \approx 0.5$ [$(P_A^{\text{S}})^2 \approx 0.5$].

As mentioned above, decays into pairs of h_{125} 's (i.e. $H \rightarrow h_{125} h_{125}$) are suppressed by alignment. To leading order in misalignment, and assuming $S_{h_{125}}^{\text{NSM}} \approx -S_H^{\text{SM}}$, the relevant coupling can be approximated as

$$\begin{aligned} g_{h_{125} h_{125} H} &\sim (S_{h_{125}}^{\text{SM}})^2 S_H^{\text{NSM}} g_{H^{\text{SM}} H^{\text{SM}} H^{\text{NSM}}} + (S_{h_{125}}^{\text{SM}})^2 S_H^{\text{S}} g_{H^{\text{SM}} H^{\text{SM}} H^{\text{S}}} \\ &\quad - S_{h_{125}}^{\text{SM}} S_{h_{125}}^{\text{NSM}} [S_{h_{125}}^{\text{SM}} g_{H^{\text{SM}} H^{\text{SM}} H^{\text{SM}}} - 2S_H^{\text{NSM}} g_{H^{\text{SM}} H^{\text{NSM}} H^{\text{NSM}}}] \\ &\quad + 2S_{h_{125}}^{\text{SM}} [(S_{h_{125}}^{\text{NSM}} S_H^{\text{S}} + S_{h_{125}}^{\text{S}} S_H^{\text{NSM}}) g_{H^{\text{SM}} H^{\text{NSM}} H^{\text{S}}} + S_{h_{125}}^{\text{S}} S_H^{\text{S}} g_{H^{\text{SM}} H^{\text{S}} H^{\text{S}}}] . \end{aligned} \quad (2.26)$$

The couplings in the first line, $g_{H^{\text{SM}} H^{\text{SM}} H^{\text{NSM}}}$ and $g_{H^{\text{SM}} H^{\text{SM}} H^{\text{S}}}$, are proportional to the entries of the mass matrix corresponding to $H^{\text{SM}} - H^{\text{NSM}}$ and $H^{\text{SM}} - H^{\text{S}}$ mixing, respectively. Thus, they vanish in the alignment limit. The contributions in the second and third line

are proportional to trilinear couplings which are not suppressed by alignment, but their respective contribution to $g_{h_{125}h_{125}H}$ all have coefficients of either $S_{h_{125}}^{\text{NSM}}$ or $S_{h_{125}}^{\text{S}}$, and are thus likewise suppressed by alignment. Hence, as noted above, $g_{h_{125}h_{125}H} = 0$ for perfect alignment.

Note that rather small departures from alignment can have considerable impact on the gluon fusion production cross section for H . At low to moderate values of $\tan\beta$, the gluon fusion production cross section is proportional to the coupling of H to pairs of top quarks, $g_{Ht\bar{t}} \propto (-S_H^{\text{NSM}}/\tan\beta + S_H^{\text{SM}})$. Thus, even relatively small variations of the value of S_H^{SM} can lead to large changes in $\sigma(ggH)$.

The mixing angle between the non SM-like states, S_H^{S} and P_A^{S} are not experimentally constrained by the observed phenomenology of h_{125} . However, large values of $(S_H^{\text{S}})^2$ and $(P_A^{\text{S}})^2$ suppress the production cross sections of H and A , respectively, and are thus challenging to probe at the LHC.

The trilinear couplings relevant for the decays ($H \rightarrow hh$), ($H \rightarrow aa$), and ($A \rightarrow ha$) are governed by free trilinear couplings between the Higgs basis interaction states and are thus not related to entries in the mass matrices. In our parameterization of the 2HDM+S, they are free parameters.

In summary, the branching ratios of ($H \rightarrow h_{125}h_{125}/ZZ/W^+W^-$) and ($A \rightarrow Zh_{125}$) decays are suppressed by the SM-like nature of h_{125} . Decays into a SM-like mode and a light non SM-like mode ($H \rightarrow h_{125}h$, $A \rightarrow h_{125}a$), or into two light non SM-like states ($H \rightarrow hh$, $H \rightarrow aa$, $H \rightarrow ha$) are not suppressed and can potentially have large branching ratios in the 2HDM+S. The detailed discussion of the various couplings and branching ratios can be found in Ref. [1]. In the following we will present benchmark scenarios optimizing all three types of decays.

As discussed above, we consider the low to moderate $\tan\beta$ regime here, in particular we fix $\tan\beta = 2.5$ for all benchmark scenarios. The dominant production mechanism for the Higgs bosons at the LHC is then gluon fusion, which we will focus on in the following. Note in particular that vector-boson-fusion production of the non SM-like Higgs bosons is suppressed by approximate alignment. This is because of the Higgs basis interaction eigenstates, only H^{SM} couples to pairs of massive vector bosons at tree level. Further, the benchmarks presented here are meant to portray only the prospects of exploring the 2HDM+S parameter space using double Higgs production. The regions displayed do not take into account bounds/projections for direct searches for additional Higgs bosons beyond h_{125} , such as ($gg \rightarrow \Phi_i \rightarrow \tau\tau$) etc.

Finally, we observe that while in 2HDM's A and H are approximately mass degenerate, their masses are a priori less tightly correlated in the 2HDM+S. For example, large mass splittings can be achieved via different mixing angles S_H^{S} and P_A^{S} . Hence when showing the planes for the benchmark scenarios, we show the effect of varying both m_A and m_H independently as labeled on the plots.

Computations of the cross sections for the benchmark values for the 2HDM+S make use of gluon fusion Higgs production cross sections and SM Higgs branching ratios taken from

Ref. [14], which we rescale by the appropriate mixing angles and $\tan\beta$.¹ For the NMSSM benchmarks, particle spectra, reduced couplings, and branching ratios are computed with `NMSSMTools` [26–30].

2.1 Z-Phobic Scenarios:

In this sections, we propose benchmark scenarios for $(gg \rightarrow \Phi_i \rightarrow \Phi_j \Phi_k)$ production at the LHC. By choosing relatively small mixing angles between the non SM-like states, $\{(S_H^S)^2, (P_A^S)^2\} \ll 1$, we consider a region of parameter space where $(\Phi_i \rightarrow Z\Phi_j)$ decays are suppressed and hence $(\Phi_i \rightarrow \Phi_j \Phi_k)$ is enhanced. We dub these the *Z-Phobic scenarios*.

Further, we assume perfect alignment, forbidding decays such as $(H \rightarrow h_{125}h_{125})$ and $(A \rightarrow Zh_{125})$. Note that deviations from perfect alignment to a degree allowed by current data would have only minor impact on the decays of the heavy Higgs bosons into non SM-like states, but as mentioned previously could impact the gluon fusion production cross section of H in a relevant way. We will show production cross sections at the LHC as well as projections for the reach with 300fb^{-1} of data in various planes of interest in the parameter space.

The projected sensitivity of the LHC for the decays $(H \rightarrow h_{125}h)$ and $(A \rightarrow h_{125}a)$ depends on the final state decay of h/a . Assuming perfect alignment, the decays of h/a into SM fermions proceed via their NSM components, and for low values of $\tan\beta$ are close to what is expected of a SM-like Higgs of the same mass. However, if there are additional Majorana fermions χ_i , e.g. dark matter candidates, which couple to the Higgs bosons via a coupling $g_{\Phi_i \chi_j \chi_k}$

$$\mathcal{L} \supset \frac{g_{h_i \chi_j \chi_k}}{2(1 + \delta_{jk})} h_i \bar{\chi}_j \chi_k + \frac{g_{a_i \chi_j \chi_k}}{2(1 + \delta_{jk})} a_i \bar{\chi}_j \gamma_5 \chi_k, \quad (2.27)$$

a and h could decay invisibly. The corresponding partial width is given by

$$\Gamma(\Phi_i \rightarrow \chi_j \chi_k) = \left(\frac{2}{1 + \delta_{ij}} \right) \frac{g_{\Phi_i \chi_j \chi_k}^2}{16\pi} m_{\Phi_i} \left[1 - \frac{(m_{\chi_j} + m_{\chi_k})^2}{m_{\Phi_i}^2} \right]^{(1+\gamma)} \left[1 - \frac{(m_{\chi_j} - m_{\chi_k})^2}{m_{\Phi_i}^2} \right]^{(1-\gamma)}, \quad (2.28)$$

where $\gamma = 1/2$ ($\gamma = -1/2$) for a CP-even (CP-odd) Φ_i . Here, we will present two scenarios: Either, we choose $g_{h\chi_1\chi_1} = g_{a\chi_1\chi_1} = 0$, which can also be interpreted as a “pure” 2HDM+S without additional states χ_i , or, we choose $g_{h\chi_1\chi_1} = g_{a\chi_1\chi_1} = 2.5 \approx \sqrt{2\pi}$ close to the largest values allowed by perturbativity, such that $(h \rightarrow \chi_1\chi_1)$ and $(a \rightarrow \chi_1\chi_1)$ will be the dominant decay mode of h and a .² Note that for the purposes of this note, we treat

¹We use the NNLO+NNLL YR4 BSM 13 TeV cross sections [14] as input, which we rescale by the appropriate mixing angles and $\tan\beta$. We have cross-checked the numerical results with an implementation of the 2HDM+S in `SusHi-1.7.0` [15–25]. For CP-even states our rescaled cross sections agree with the `SusHi` results within a few percent, an error much smaller than the renormalization and matching scale uncertainties. For CP-odd states, we found differences as large as $\sim 10 - 20\%$. This is due to our rescaling using leading-order loop factors for the conversion to the CP-odd gluon fusion cross section, cf. Ref. [1].

²The couplings of the remaining mass eigenstates, h_{125} , H , and A , to additional fermions χ_i are set to zero throughout this note.

the $g_{\Phi_i \chi_j \chi_k}$ as free parameters, see e.g. Ref. [31] for a discussion of such couplings in the context of consistent dark matter phenomenology.

In the first two columns of Table 1 we present benchmark scenarios for $(H \rightarrow h_{125}h)$ and $(A \rightarrow h_{125}a)$ resonant production. Depending on the couplings $g_{\Phi_i \chi_1 \chi_1}$, these scenarios result in the daughter Higgs bosons decaying either visibly ($2b$) or invisibly (\cancel{E}_T). We set all the free trilinear couplings between the interaction states, listed in Eq. (2.12), to zero, cf. the discussion below Eq. (2.22). The third column corresponds to a scenario where we choose non-zero values for the free trilinear couplings, in particular $g_{H^{\text{NSM}} H^S H^S}$, $g_{H^{\text{NSM}} A^S A^S}$, and $g_{H^S A^{\text{NSM}} A^S}$, which are most relevant for $(H \rightarrow hh)$, $(H \rightarrow aa)$, and $(A \rightarrow ha)$ decays, respectively. For this latter benchmark, we do not include the decays of h and a in the results presented here, thus, there is no need to fix the couplings of h and a to χ_1 .

We have chosen heavy Higgs bosons with masses of 700 GeV, such that they are heavy enough to have evaded detection so far, but are light enough to have sizable production cross section at the 13 TeV LHC. The singlet components for both of them, $(S_H^S)^2$ and $(P_A^S)^2$, are fixed to 0.1, such that the gluon fusion production cross section is not unduly suppressed and decays into Z are disfavored. For the low values of $\tan \beta$ considered here, the dominant decay mode for the heavy Higgs bosons out of the decays into pairs of SM particles would be to $t\bar{t}$, which is challenging to probe at the LHC [32–39]. The masses of the mostly singlet-like a and h are set to 200 GeV, light enough for the heavy Higgs bosons to readily decay to them. The mass of the additional dark matter candidate χ_1 is set to 50 GeV. The trilinear couplings are not expected to be relevant unless very large, as can be seen from Eq. (2.22), hence we set them to 0 for the first two benchmarks.

2.1.1 Z-Phobic: $h_{125} + \text{Visible}$ ($H \rightarrow h_{125}a$ and $A \rightarrow h_{125}h$)

In Figs. 2 and 4 we show the variation in the final state cross-section when changing the values of the parameters listed in Table 1. Here and in all the plots, the parameters held fixed to benchmark values are portrayed in each plot label. The coupling of h/a to possible dark matter particles χ_1 is set to 0, hence, this benchmark scenario can also be interpreted as a “pure” 2HDM+S without the addition of the state χ_1 . The contours and color shading show the cross-section, and the gray shaded region denotes the region where the LHC is expected to probe this scenario with 300 fb^{-1} of data in the $4b$ channel; we take the projected sensitivity from Ref. [40]. The dashed black lines denote cross-sections which are a factor of two smaller than the projected reach. The sensitivity in the $2b2\gamma$ channel is expected to be similar [40]. Note that the cross sections shown in the figures do not include h_{125} branching ratios, which are taken to be the SM values, hence sensitivities for different h_{125} decay modes can be easily compared. The red stars denote the benchmark point defined in Table 1. Note that we treat the sensitivities independently for H and A .

In Fig. 2 we show the variations in $(gg \rightarrow A \rightarrow h_{125}a)$ and in Fig. 3 the most relevant branching ratios for this channel. The most relevant quantities for this cross-section are the pseudoscalar mixing angle and masses shown in the two top left panels. The observed strong suppression for maximally mixed $A^{\text{NSM}} - A^S$ originates from the suppression of the relevant trilinear coupling in that region, cf. Eq. (2.22). The main effect of varying m_A is in the gluon fusion production cross section, which results in an overall scaling of the

Z-Phobic	Visible (2b)	Invisible (\cancel{E}_T)	Double Singlet
m_H [GeV]		700	
m_A [GeV]		700	
m_h [GeV]		200	
m_a [GeV]		200	
m_χ [GeV]		50	
$\tan \beta$		2.5	
$(S_H^S)^2$		0.1	
$(P_A^S)^2$		0.1	
$g_{\Phi_i \chi_1 \chi_1}$	0	2.5	—
$g_{H^{\text{NSM}} H^S H^S}$ [GeV]		0	174
$g_{H^{\text{NSM}} A^S A^S}$ [GeV]		0	174
$g_{A^{\text{NSM}} H^{\text{NSM}} H^S}$ [GeV]		0	174
$\sigma(ggH)$ [pb]		0.13	
$\sigma(ggA)$ [pb]		0.19	
$\text{BR}(H \rightarrow h_{125} h)$		0.30	0.29
$\text{BR}(H \rightarrow hh)$		0	0.0094
$\text{BR}(H \rightarrow aa)$		0	0.0094
$\text{BR}(H \rightarrow Za)$		0.45	0.44
$\text{BR}(A \rightarrow h_{125} a)$		0.28	0.27
$\text{BR}(A \rightarrow ha)$		0	0.018
$\text{BR}(A \rightarrow Zh)$		0.42	0.41
$\text{BR}(h \rightarrow \chi_1 \chi_1)$	0	1.00	—
$\text{BR}(h \rightarrow b\bar{b})$	0.94	0.00	—
$\text{BR}(a \rightarrow \chi_1 \chi_1)$	0	1.00	—
$\text{BR}(a \rightarrow b\bar{b})$	0.94	0.00	—

Table 1: Z-Phobic benchmark scenarios. Perfect alignment is assumed, and all free trilinear couplings not listed above, cf. Eq. (2.12), are set to 0.

cross sections shown. We further note that the LHC loses sensitivity as a approaches the $t\bar{t}$ threshold. Above the top threshold and for low values of $\tan \beta$, a will decay preferentially to top quark pairs, cf. Fig. 3. It is interesting to note that in such a case, the final state signature will be $t\bar{t}h_{125}$, and the cross section may be of the same order as the $t\bar{t}h_{125}$ associated production cross section in the SM. To the best of our knowledge, no projections exist for this final state. However, it seems possible to get stringent constraints in this case by demanding that the top pairs reconstruct to m_a , combined with the demand that $m_a + m_{h_{125}} = m_A$.

The dependence on the scalar mixing angles and masses is due to the correlated decays of $(A \rightarrow Zh/H)$, cf. Fig. 3. Since the coupling $(A \rightarrow Zh/H)$ is proportional to the NSM component of h/H , cf. Eq. (2.17), the observed decrease in sensitivity for $(A \rightarrow h_{125}a)$ with increasing NSM component of the scalars can be easily understood. Similarly, as the h/H

become heavier, Zh/H channels are not kinematically accessible, and hence the sensitivity for $(A \rightarrow h_{125}a)$ increases. Therefore, the dark regions shown in the bottom four panels and top two right panels of Fig. 2 should be understood to denote regions mainly driven by where the $(A \rightarrow Zh/H)$ decay is sufficiently suppressed so as to not impact the sensitivity to the $(A \rightarrow h_{125}a)$ channel.

Fig. 4 shows the variations in $(gg \rightarrow H \rightarrow h_{125}h)$ and Fig. 5 the most relevant branching ratios. The same qualitative behavior for the cross-sections and LHC sensitivities is observed as in Fig. 2, with the obvious interchange of the masses and mixing angles for the scalars and pseudoscalars. The overall reduction in LHC sensitivities/cross sections can be understood from the fact that even for $m_A = m_H$, the gluon fusion production cross section for the scalar H can be almost a factor of 2 smaller than the production cross section for the pseudoscalar A .

As can be seen from these plots, the LHC will be sensitive to large regions of the parameter space in this scenario, even with only 300 fb^{-1} of data. However, we stress that whereas more data will certainly lead to the exploration of a larger region of allowed parameters, to optimize coverage, complimentary and correlated search channels such as $(A \rightarrow Zh)$ and $(H \rightarrow Za)$ should be utilized as well.

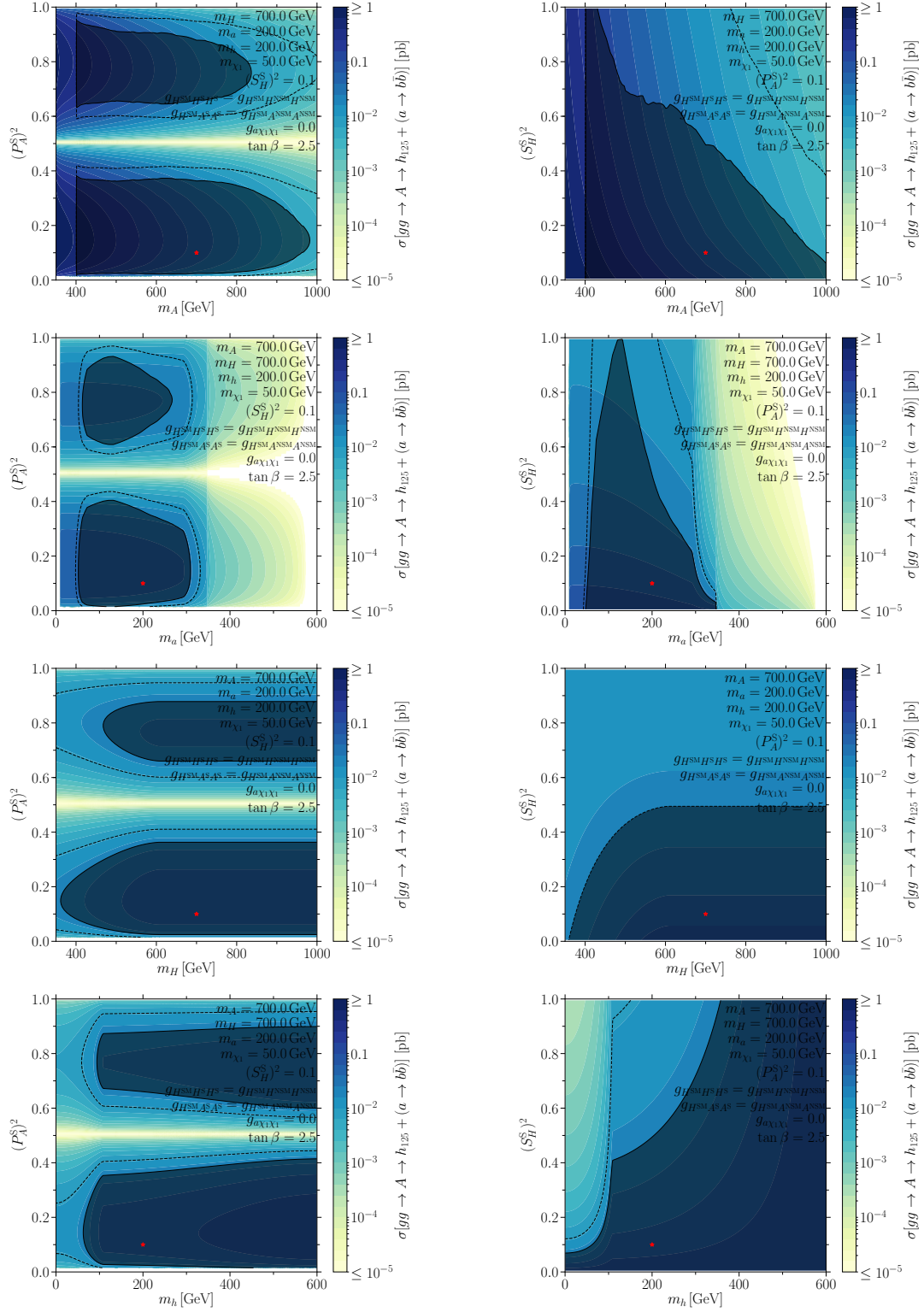


Figure 2: Cross sections and projected LHC sensitivities with 300 fb^{-1} of data for $(gg \rightarrow A \rightarrow h_{125}a \rightarrow 4b)$ in the planes of the relevant masses and mixing angles. The color scale and contours denote cross-sections as labeled by the color bars. The dark shaded regions denote the region where the cross section is larger than the projected sensitivity of the LHC. The dashed black lines denote cross sections a factor of two smaller. The red stars indicate the benchmark point from the first column in Table 1.

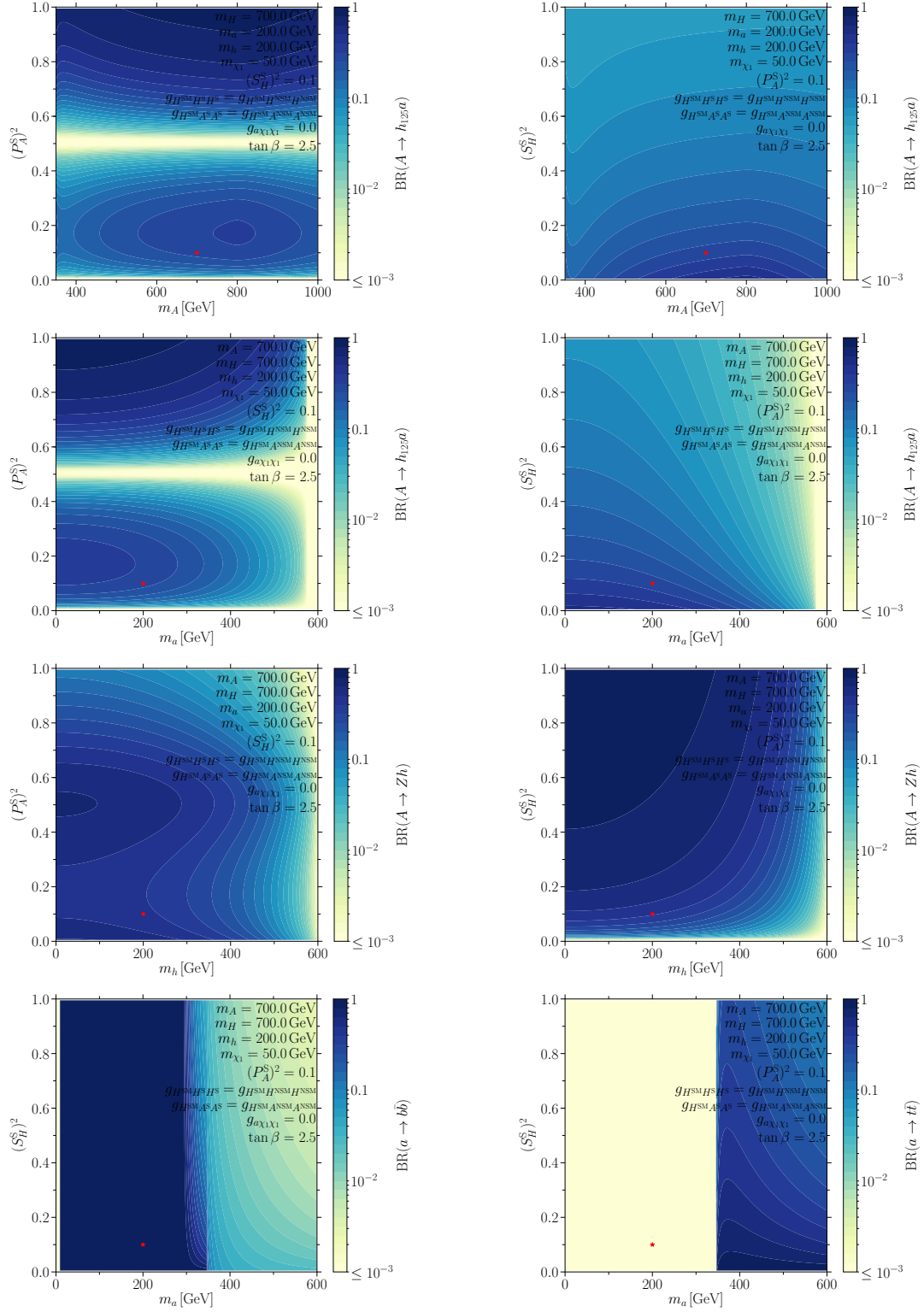


Figure 3: Most relevant branching ratios for $(gg \rightarrow A \rightarrow h_{125}a \rightarrow 4b)$ searches in planes of the relevant masses and mixing angles. The color scale denotes cross-sections as labeled by the color bars. The red stars indicate the benchmark point from the first column in Table 1.

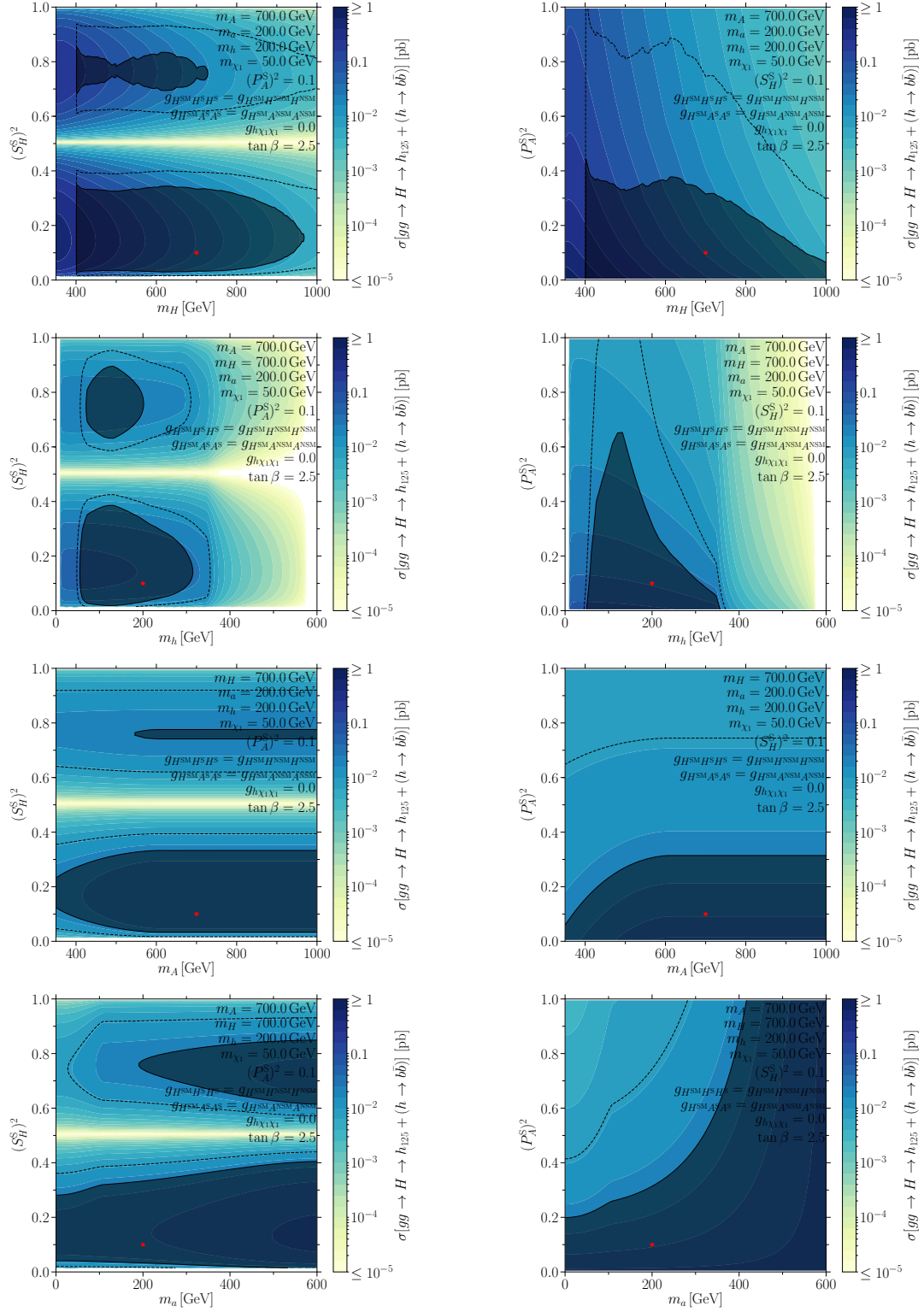


Figure 4: Cross sections and projected LHC sensitivities with 300 fb^{-1} of data for $(gg \rightarrow H \rightarrow h_{125}h \rightarrow 4b)$ in the planes of the relevant masses and mixing angles. The color scale and contours denote cross-sections as labeled by the color bars. The dark shaded regions denote the region where the cross section is larger than the projected sensitivity of the LHC. The dashed black lines denote cross sections a factor of two smaller. The red stars indicate the benchmark point from the first column in Table 1.

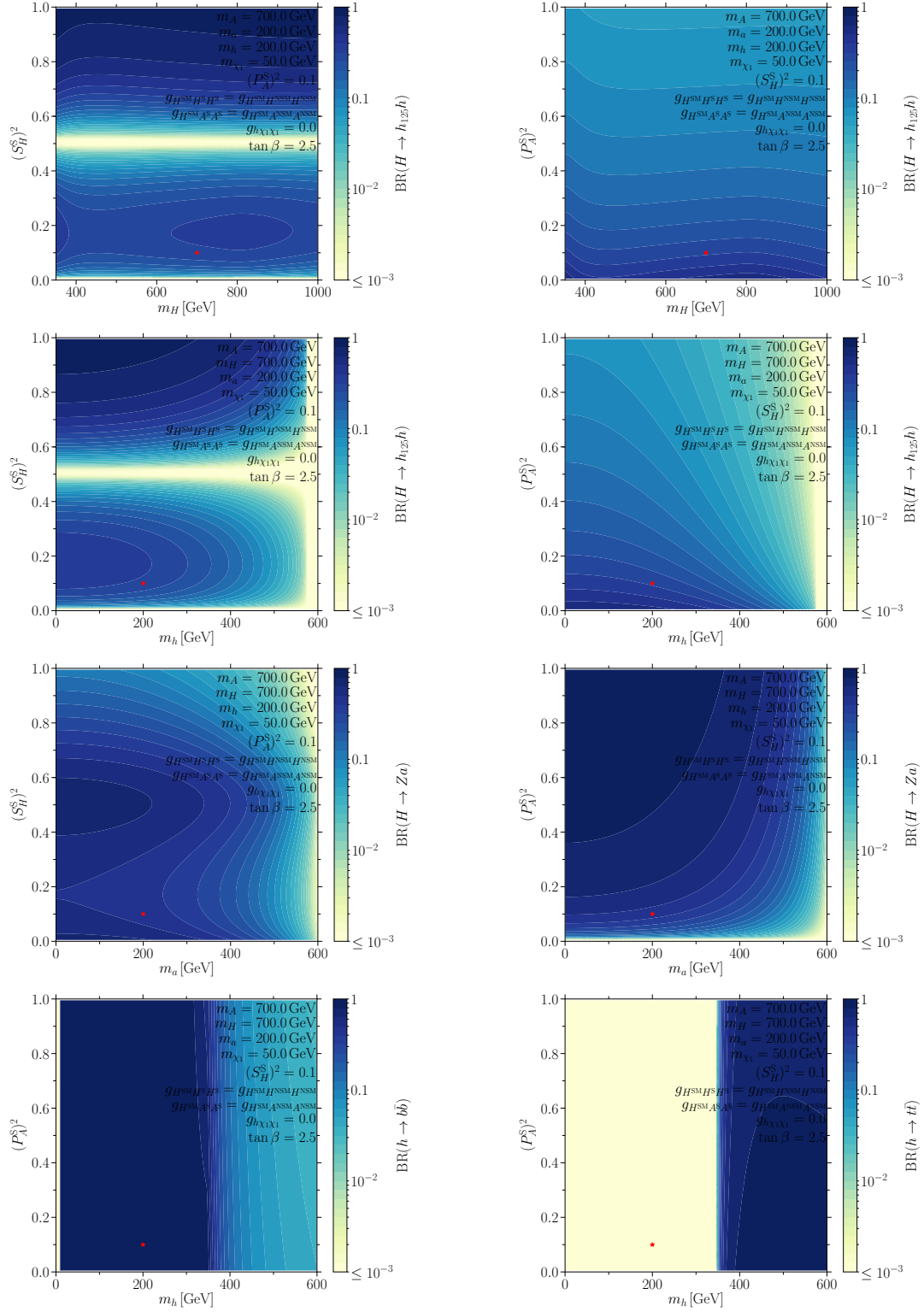


Figure 5: Most relevant branching ratios for $(gg \rightarrow H \rightarrow h_{125}h \rightarrow 4b)$ searches in planes of the relevant masses and mixing angles. The color scale denotes cross-sections as labeled by the color bars. The red stars indicate the benchmark point from the first column in Table 1.

2.1.2 Z-Phobic: h_{125} +Invisible ($H \rightarrow h_{125}a$ and $A \rightarrow h_{125}h$)

In Figs. 6 and 7 the variation in the final state cross-sections and the related LHC sensitivities, taken from Ref. [41], are portrayed for the same channels as in the previous section, but with a large values of $g_{h\chi_1\chi_1} = g_{a\chi_1\chi_1} = 2.5$, such that $\text{BR}(h/a \rightarrow \chi_1\chi_1) \approx 1$. The cross-sections shown and their behavior are very similar to what was shown/discussed in the Sec. 2.1.1. However, somewhat smaller regions of parameter space are within the projected sensitivity of the LHC. The cut-off for $m_{a/h} < 100 \text{ GeV}$ is due to the fact that we fixed $m_{\chi_1} = 50 \text{ GeV}$, hence, the decays of a/h into pairs of χ_1 are kinematically forbidden.

While the LHC sensitivity is reduced compared to the Visible scenario presented in the previous section, upcoming runs of the LHC could still probe sizable regions of this scenario's parameter space.

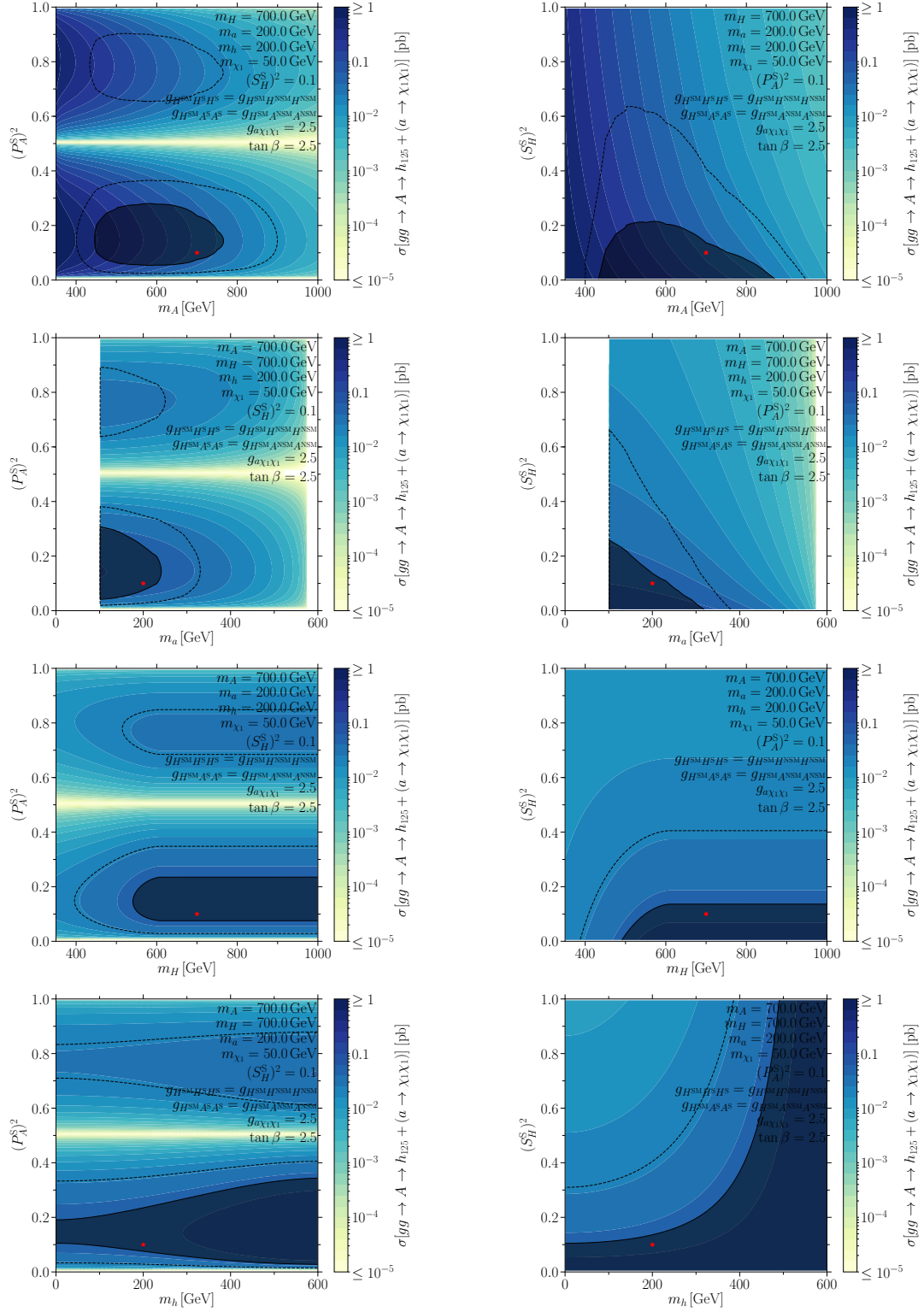


Figure 6: Cross sections and projected LHC sensitivities with 300 fb^{-1} of data for $(gg \rightarrow A \rightarrow h_{125} a \rightarrow 2b + \cancel{E}_T)$ in the planes of the relevant masses and mixing angles. The color scale and contours denote cross-sections as labeled by the color bars. The dark shaded regions denote regions where the cross sections exceeds the projected LHC sensitivity. The dashed black lines denote cross sections a factor of two smaller. The red stars indicate the benchmark point from the second column in Table 1.

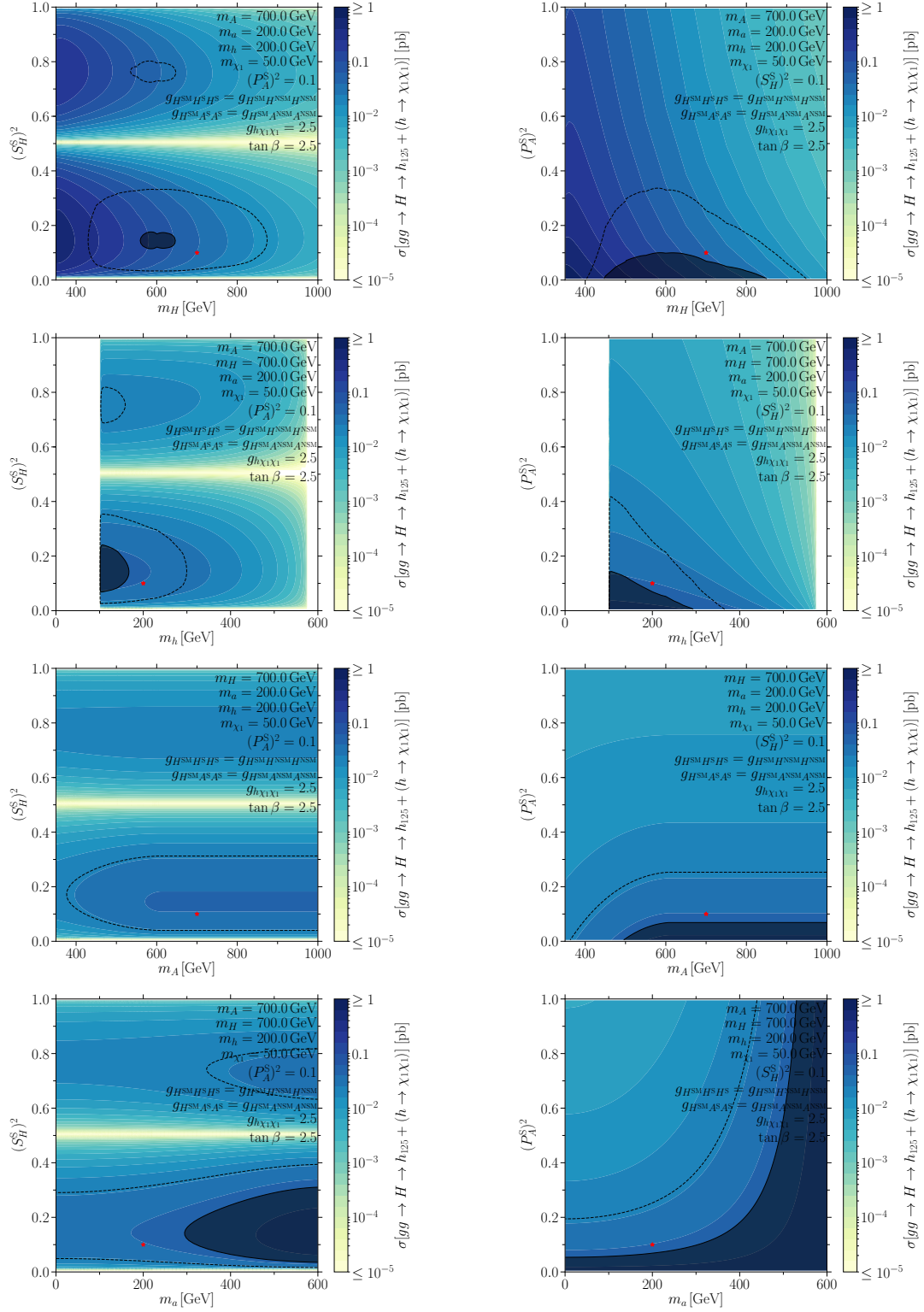


Figure 7: Cross sections and projected LHC sensitivities with 300 fb^{-1} of data for $(gg \rightarrow H \rightarrow h_{125}h \rightarrow 2b + \cancel{E}_T)$ in the planes of the relevant masses and mixing angles. The color scale and contours denote cross-sections as labeled by the color bars. The dark shaded regions denote regions where the cross sections exceeds the projected LHC sensitivity. The dashed black lines denote cross sections a factor of two smaller. The red stars indicate the benchmark point from the second column in Table 1.

2.1.3 Z-Phobic: Double Singlet Scenario ($H \rightarrow hh$, $H \rightarrow aa$, and $A \rightarrow ha$)

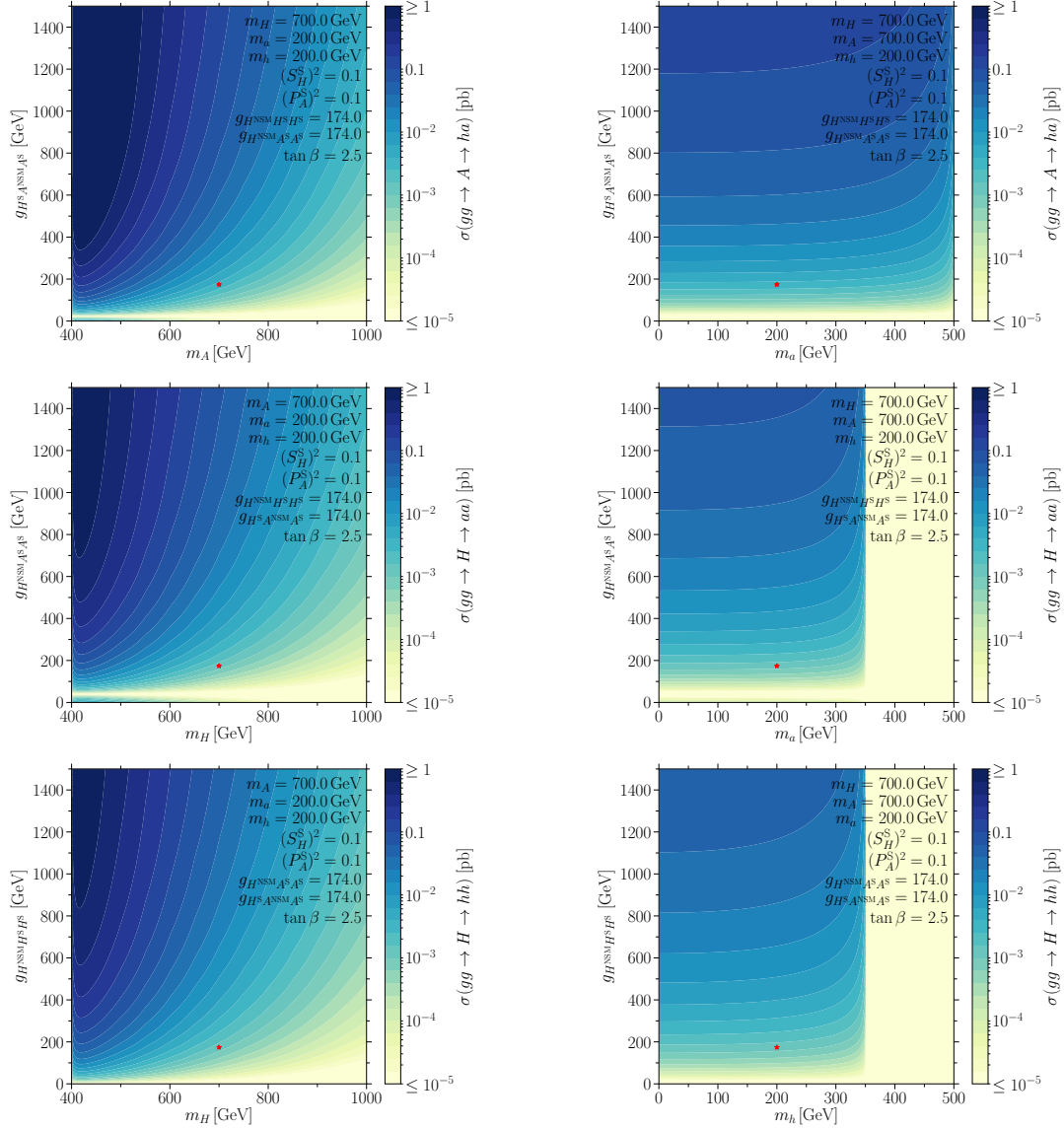


Figure 8: Cross sections as denoted by color bars for ($gg \rightarrow A \rightarrow ha$; first row), ($gg \rightarrow H \rightarrow aa$; second row), and ($gg \rightarrow H \rightarrow hh$; third row) in the planes of the most relevant masses and trilinear couplings. The red stars indicate the benchmark point from the third column in Table 1.

To the best of our knowledge, no projections for the sensitivity of resonant hh , aa , or ha production exist. Hence, we present only the cross section for our benchmark scenario here. We have chosen conservative values for the trilinear couplings. We show the variation in the cross-section as a function of the most relevant couplings and masses for each of these channels in Fig. 8. The three rows in the figure denote the three different channels. We have not taken into account the branching ratios of the daughter states h or a , since these

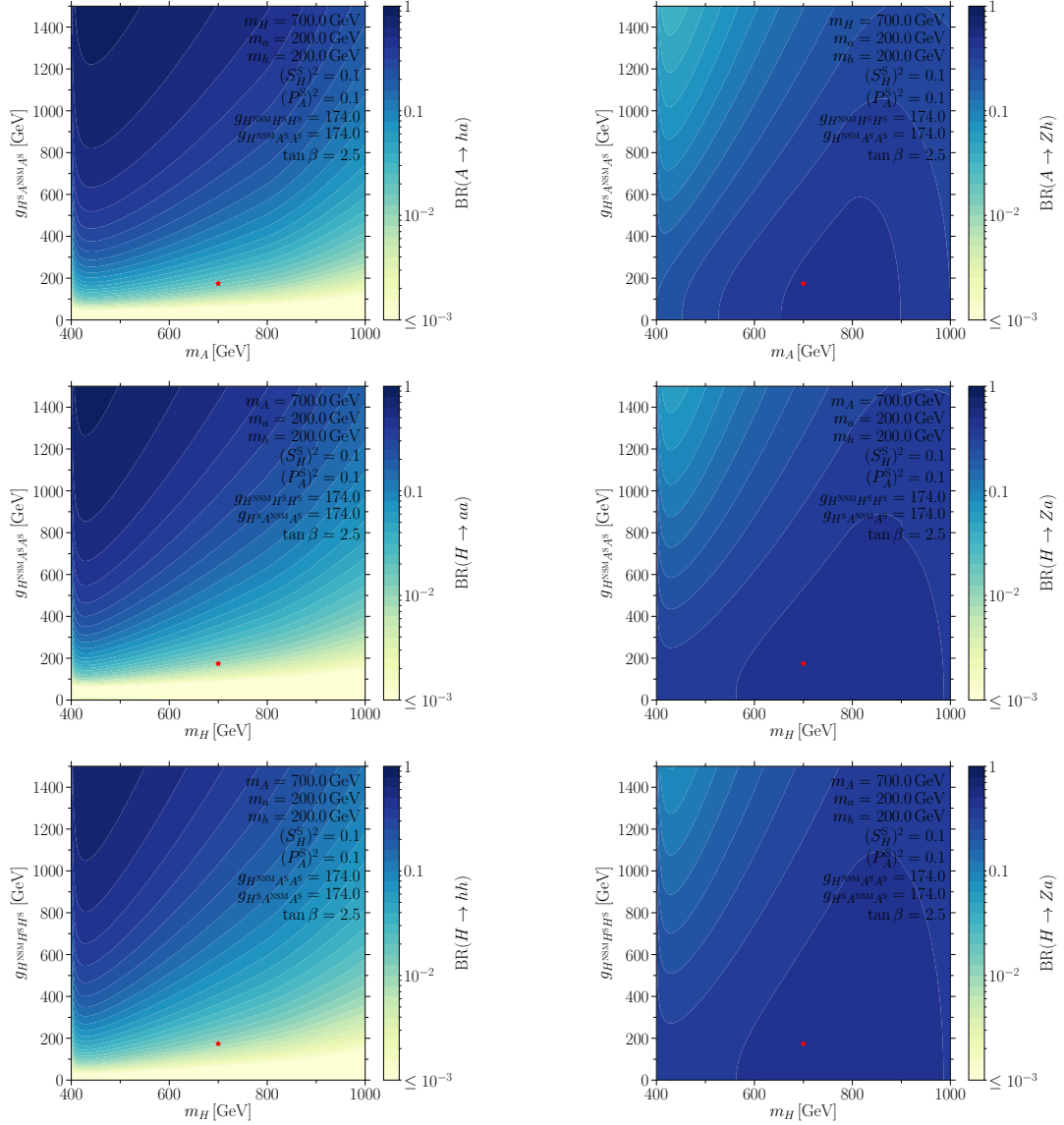


Figure 9: Most relevant branching ratios for $(A \rightarrow ha)$; first row), $(H \rightarrow aa)$; second row), and $(H \rightarrow hh)$; third row) searches in the planes of the most relevant masses and trilinear couplings. The red stars indicate the benchmark point from the third column in Table 1.

are arbitrarily controlled by the possibility of decays into missing energy.

Note that unlike $(H \rightarrow h_{125}h)$ and $(A \rightarrow h_{125}a)$ discussed previously, the decays $(H \rightarrow hh)$, $(H \rightarrow aa)$, and $(A \rightarrow ha)$ considered here are essentially governed by the free trilinear couplings between the Higgs basis interaction states as well as the masses of the particles involved in each process. In Fig. 9 we show the most relevant branching ratios for such processes. For each channel (i.e. the different rows), we show the branching ratio corresponding to the signal channel in the left panel, while the right panel shows the corresponding branching ratio into a Z boson and an h or a .

From Fig. 8 we see that the production cross-section for these channels can easily be $\mathcal{O}(100)$ fb, which may be explored at the LHC.

2.2 Max Misalignment Scenario: $H \rightarrow h_{125}h_{125}$

m_H [GeV]	700			
m_A [GeV]	1000			
m_h [GeV]	$m_H - 100$ GeV = 600			
m_a [GeV]	950			
$S_{h_{125}}^{\text{NSM}}$	0.2	0.2	-0.2	-0.2
$S_{h_{125}}^{\text{S}}$	0.5	-0.5	0.5	-0.5
S_H^{S}	0.3			
$g_{H^{\text{SM}}H^{\text{SM}}H^{\text{SM}}} = 3\mathcal{M}_{S,11}^2/\sqrt{2}v$ [GeV]	1800	1400	1400	1800
$g_{H^{\text{SM}}H^{\text{SM}}H^{\text{NSM}}} = 3\mathcal{M}_{S,12}^2/\sqrt{2}v$ [GeV]	1500	480	-480	-1500
$g_{H^{\text{SM}}H^{\text{SM}}H^{\text{S}}} = \mathcal{M}_{S,13}^2/\sqrt{2}v$ [GeV]	340	-680	680	-340
$g_{H^{\text{SM}}H^{\text{NSM}}H^{\text{S}}} = \mathcal{M}_{S,23}^2/\sqrt{2}v$ [GeV]	-560	-370	-370	-560
$\sigma(ggH)$ [pb]	0.96	0.018	0.36	0.097
$\text{BR}(H \rightarrow h_{125}h_{125})$	0.032	0.35	0.15	0.016
$\text{BR}(H \rightarrow ZZ)$	0.23	0.20	0.13	0.31
$\text{BR}(H \rightarrow WW)$	0.46	0.40	0.26	0.63

Table 2: Benchmark Scenario for $(gg \rightarrow H \rightarrow h_{125}h_{125})$ resonant h_{125} pair production. Of the parameters not listed, $\tan\beta = 2.5$, and all free trilinear couplings, cf. Eq. (2.12) are set to 0. The relevant trilinear couplings are computed from the scalar squared mass matrix, \mathcal{M}_S^2 , obtained from the given values of the masses and mixing angles.

In this section, we present benchmark scenarios for resonant pair production of SM-like Higgs bosons in the 2HDM+S. Note that here we compare the production cross section to *current* exclusion limits from the 13 TeV LHC in the $4b$ final state taken from Refs. [42–45] and in the $2b2\gamma$ final state taken from Refs. [46–48]. Projections for 300 fb^{-1} may be obtained by rescaling the limit with the increased luminosity. In the CP-conserving 2HDM+S, the only resonant production mechanisms at the LHC are $(pp \rightarrow H \rightarrow h_{125}h_{125})$ and $(pp \rightarrow h \rightarrow h_{125}h_{125})$. We focus on the former process, benchmark scenarios for the latter channel can be obtained by interchanging the values of the relevant mixing angles. The SM production of h_{125} pairs (including interference effects) is not expected to be relevant in the region of parameter space considered here.

As discussed in Sec. 2, the branching ratios of H and h into pairs of SM-like Higgs states are suppressed by the proximity to alignment. For our benchmark scenario, we consider the most optimistic case of approximately maximal misalignment allowed by current LHC constraints on the couplings of the observed SM-like state [49–53]. Approximately, these measurements allow a H^{NSM} component of $(S_{h_{125}}^{\text{NSM}})^2 \lesssim 0.05$ and a H^{S} component of $(S_{h_{125}}^{\text{S}})^2 \lesssim 0.3$. In Table 2 we show the parameters for our benchmark points. In the interest of maximizing the $(H \rightarrow h_{125}h_{125})$ cross section, we have fixed the masses of h and

a such that $(H \rightarrow hh)$, $(H \rightarrow aa)$, and $(H \rightarrow h_{125}h)$ decays are kinematically forbidden. All free trilinear couplings between the Higgs basis interaction states (i.e. those not related to mixing angles and masses) are set to 0. The dominant effect of the mixing angle S_H^S is an overall suppression of the gluon fusion production cross section of H . One expects that the mixing angle $S_{h_{125}}^S$ would have minimal effect since its main impact is to suppress the total h_{125} width, however, since the coupling $g_{h_{125}h_{125}H}$ is a sum of small factors, signs can play a very relevant role. Hence, we present benchmark scenarios for the different possible combinations of the signs of the relevant mixing angles. The mass of the heavy Higgs boson is chosen to be $m_H = 700$ GeV for reasons similar to the ones for the previous benchmarks. The mass of h for the benchmark points is chosen to be 600 GeV such that decays of H into the other Higgs channels discussed in the previous sections are forbidden. When varying m_H in the plots, m_h will be varied as $(m_h = m_H - 100 \text{ GeV})$. Note that the choice of m_h has considerable impact on the relevant trilinear couplings which are computed from the masses and mixing angles. Our choice of the masses of the pseudoscalar states ensures that $(H \rightarrow Za)$ decays (and similar channels) are kinematically forbidden, but otherwise plays no role for $(H \rightarrow h_{125}h_{125})$. Thus, we fix the masses to $m_A = 1 \text{ TeV}$ and $m_a = 950 \text{ GeV}$.

Fig. 10 demonstrates how the resonant h_{125} pair production cross section changes as a function of the mass of the non SM-like Higgs boson m_H and the relevant mixing angles. Gray regions are already excluded by current LHC data from $(gg \rightarrow H \rightarrow h_{125}h_{125})$ searches, taken from Refs. [42–48]. The dashed lines indicate where the cross section is a factor of two smaller than current limits, which may be expected to be probed with 300 fb^{-1} of data. We also indicate regions of parameter space ruled out by current searches in the $gg \rightarrow H \rightarrow ZZ$ channel [54–62] by the orange shaded regions, and regions ruled out by $(gg \rightarrow H \rightarrow WW)$ searches [63–69] by the red shaded regions. The red stars indicate the benchmark points in Table 2. Depending on the relative signs of the mixing angles, the benchmark points may either be already marginally excluded (top and bottom panels on the right), or, may be challenging to probe even with high luminosity. It is interesting to note that for some regions of parameter space, bounds from resonant h_{125} pair production give stronger constraints on the mixing angles of h_{125} than the precision measurements of the production cross sections and branching ratios of h_{125} . We also stress that decays of $(H \rightarrow ZZ/W^+W^-)$ are only proportional to the SM component of H and hence directly to $S_{h_{125}}^{\text{NSM}}$. Therefore more robust constraints on the misalignment of h_{125} could be obtained by combining such searches. We show the most relevant branching ratios of H in the m_H – $S_{h_{125}}^{\text{NSM}}$ plane in Fig. 11, and in the m_H – S_H^S plane in Fig. 12.

In Fig. 13 we show the production cross section together with the constraints from current $(gg \rightarrow H \rightarrow h_{125}h_{125})$, $(gg \rightarrow H \rightarrow ZZ)$, and $(gg \rightarrow H \rightarrow WW)$ searches together with the most relevant branching ratios of H and h_{125} in the plane of the H^S and H^{NSM} component of the SM-like mass eigenstate h_{125} .

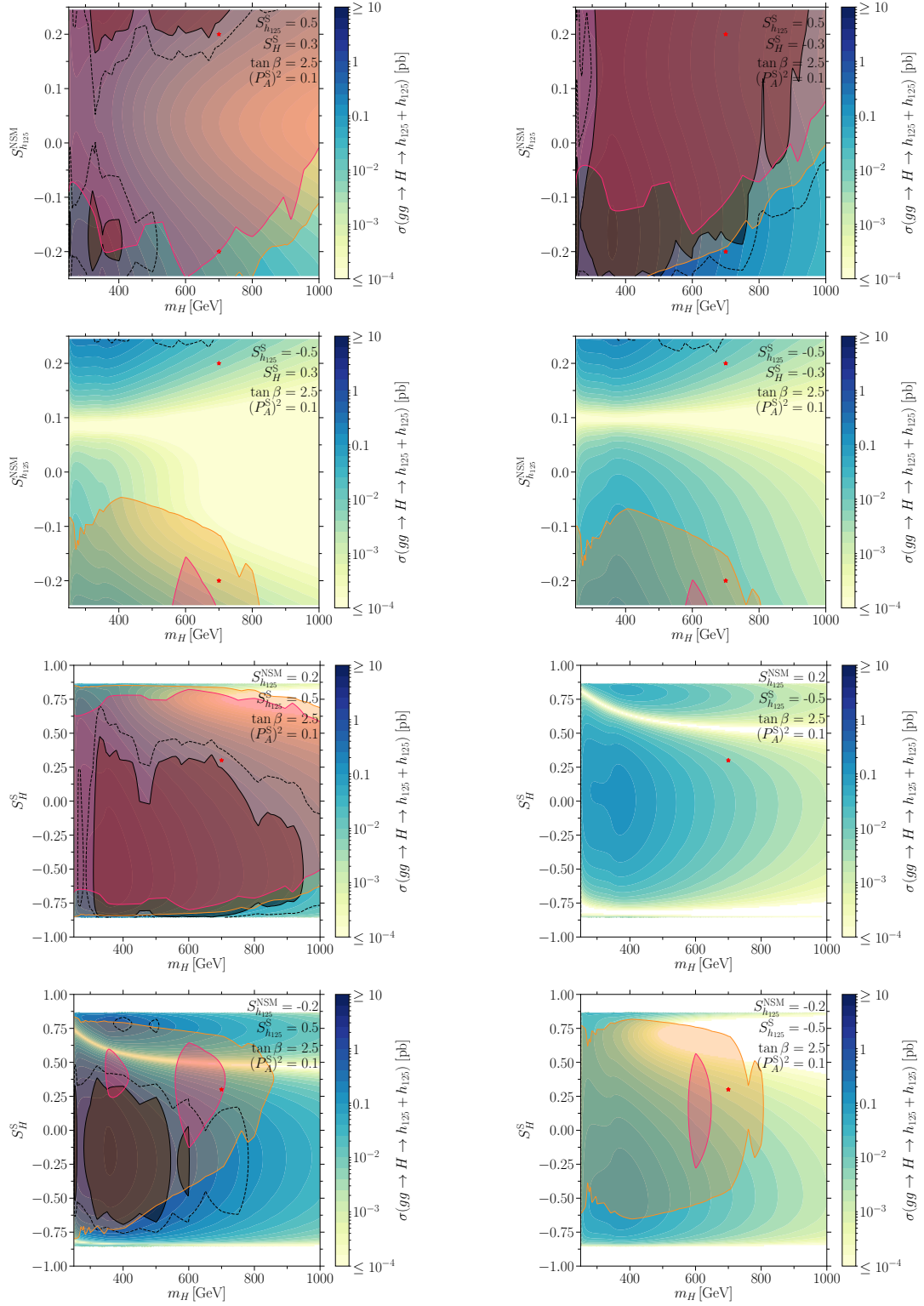


Figure 10: Production cross section and current LHC limits for $(gg \rightarrow H \rightarrow h_{125}h_{125})$ in the plane of the heavy Higgs boson m_H and various relevant mixing angles. The colored contours denote the total cross-section according to the color bar label. Gray shaded regions are excluded by current $(gg \rightarrow H \rightarrow h_{125}h_{125})$ LHC searches. Black dashed lines label cross sections which are a factor two smaller than the current sensitivity, and hence may be expected to be probed with 300 fb^{-1} of data. Red [orange] shaded area denote regions ruled out by current $(gg \rightarrow H \rightarrow W^-W^-) [(gg \rightarrow H \rightarrow ZZ)]$ LHC searches. The red stars indicate the benchmark points presented in Table 2.

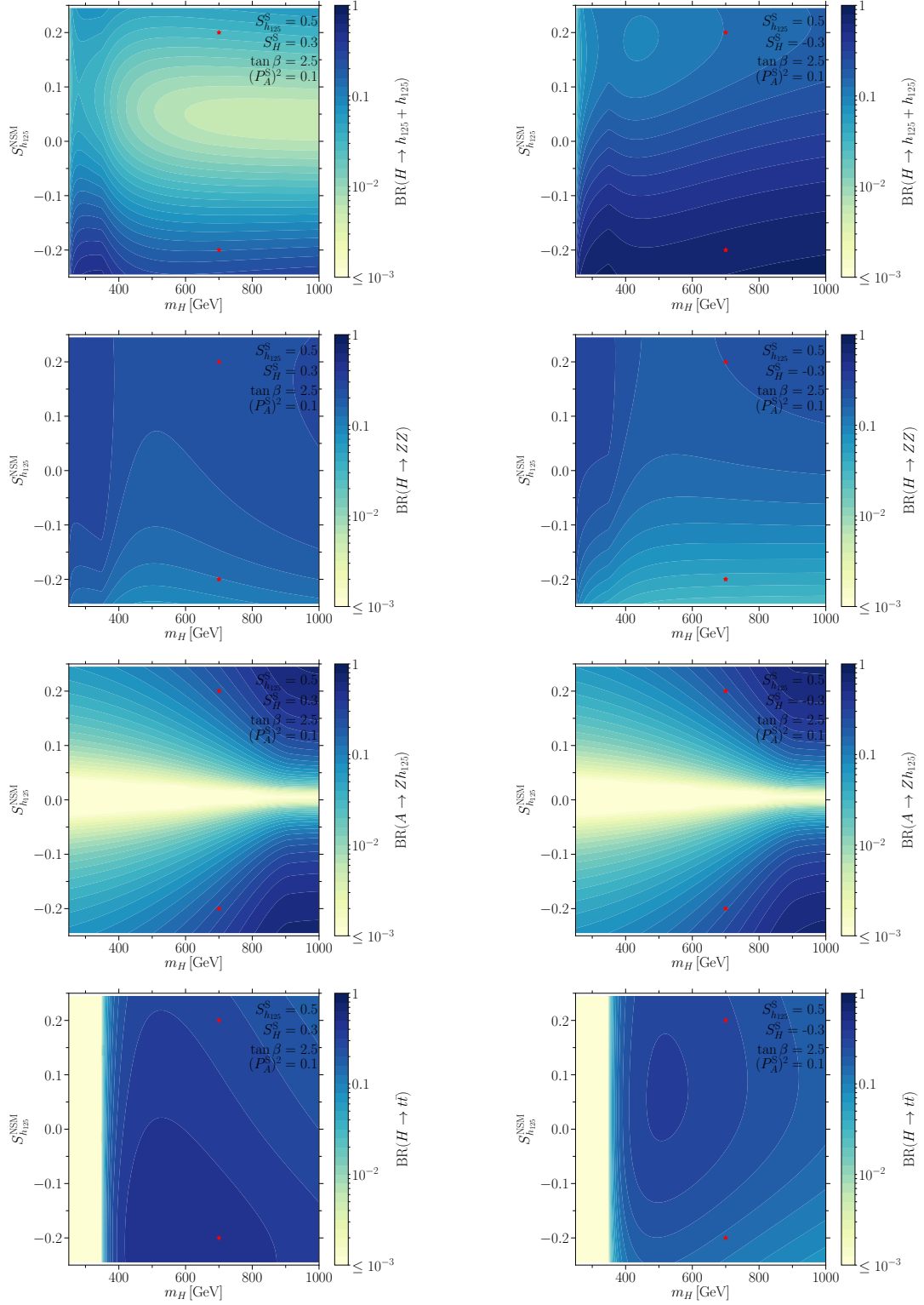


Figure 11: Most relevant branching ratios as labeled by the colorbar for $(gg \rightarrow H \rightarrow h_{125}h_{125})$ searches in the m_H - $S_{h_{125}}^{\text{NSM}}$ plane. For all plots $S_{h_{125}}^S = 0.5$. For plots in the left column $S_{h_{125}}^S = 0.3$, while in the right column $S_{h_{125}}^S = -0.3$. The red stars indicate the benchmark points presented in Table 2. Note that we do not show the $(H \rightarrow WW)$ branching ratio, its scaling with the mass and the mixing angle is identical to $\text{BR}(H \rightarrow ZZ)$.

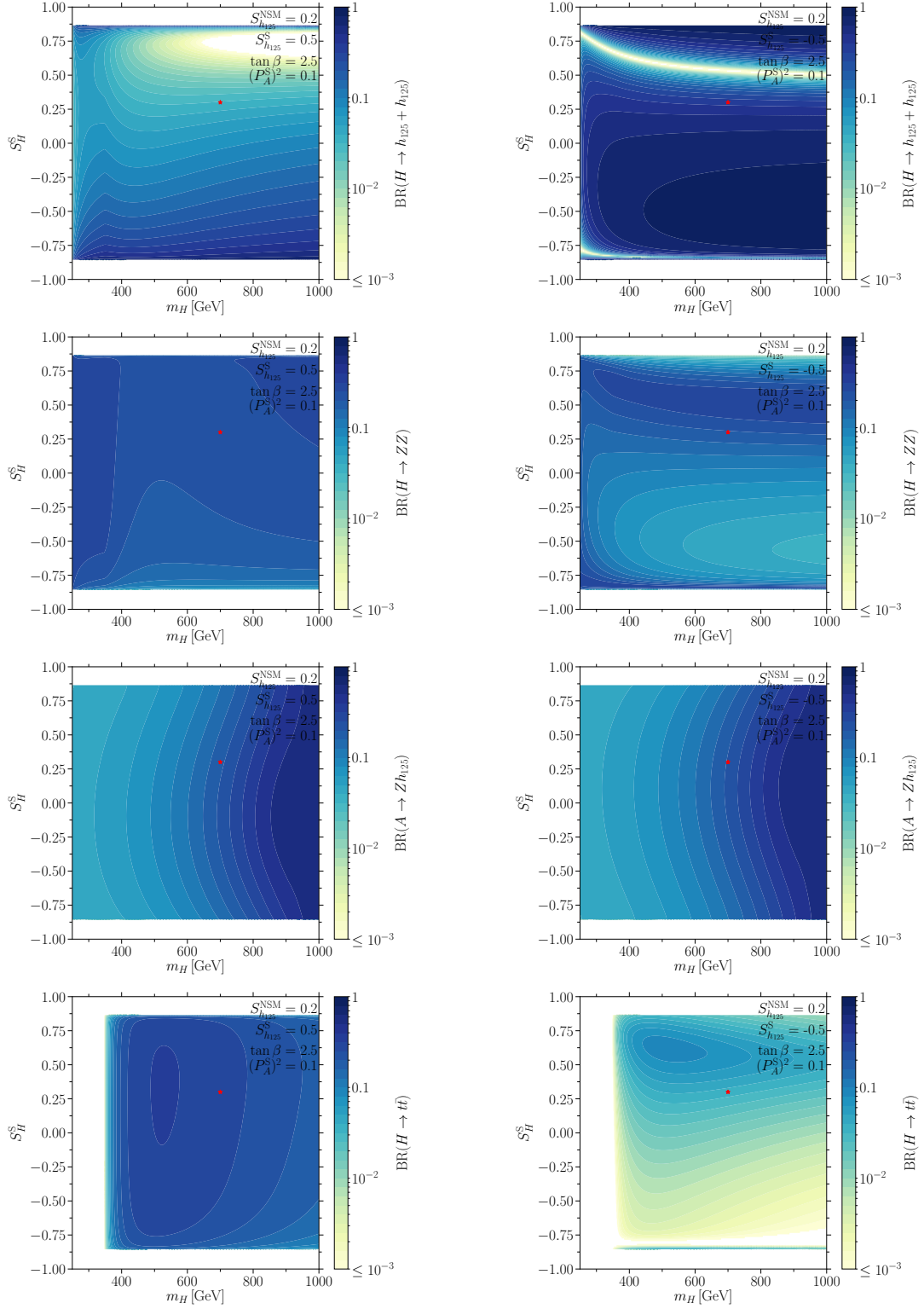


Figure 12: Most relevant branching ratios as labeled by the colorbar for $(gg \rightarrow H \rightarrow h_{125}h_{125})$ searches in the m_H - S_H^S plane. For all plots $S_{h_{125}}^{NSM} = 0.2$. For plots in the left column $S_{h_{125}}^S = 0.5$, while in the right column $S_{h_{125}}^S = -0.5$. The red stars indicate the benchmark points presented in Table 2. Note that we do not show the $(H \rightarrow WW)$ branching ratio, its scaling with the mass and the mixing angle is identical to $BR(H \rightarrow ZZ)$.

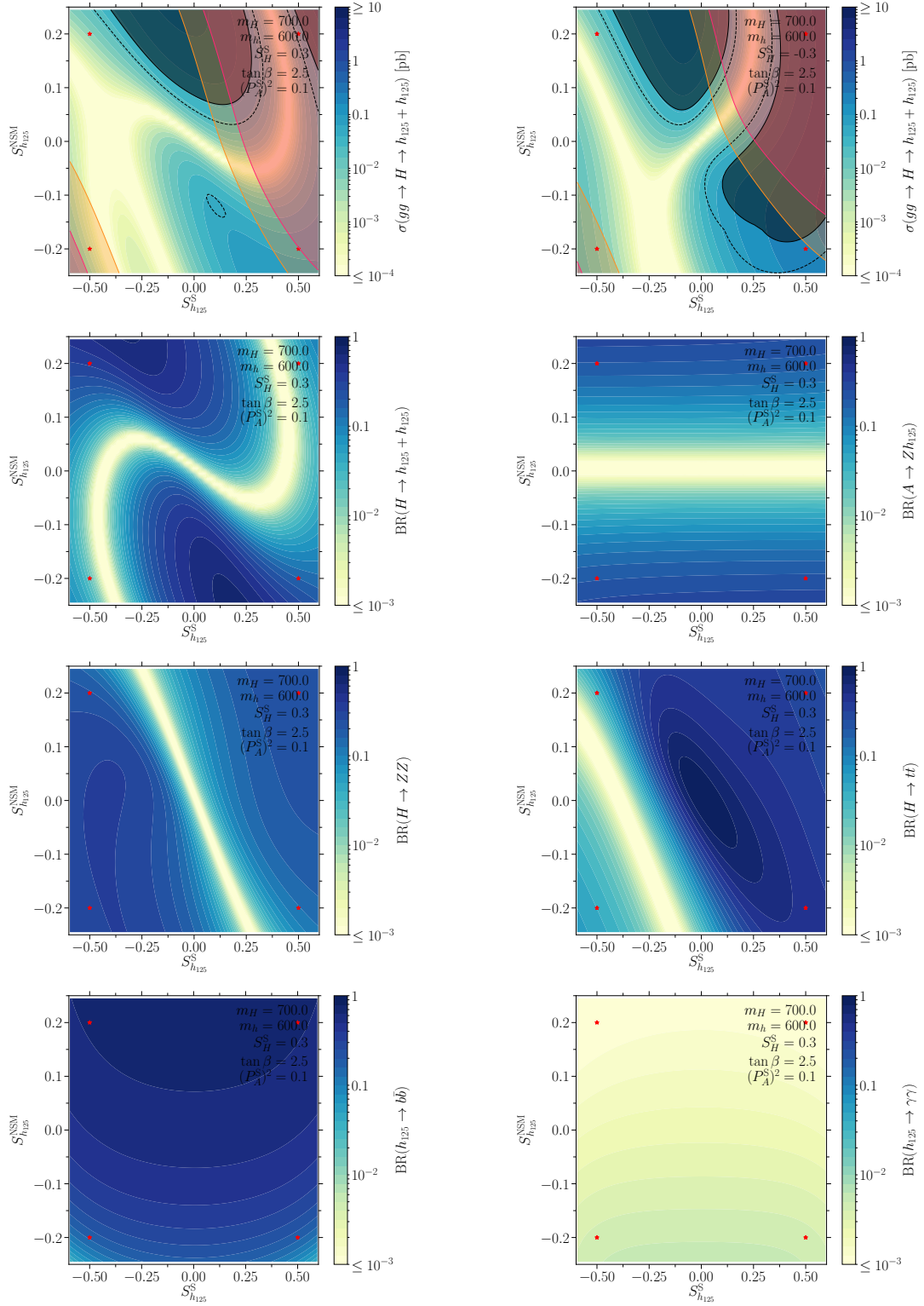


Figure 13: *Top row:* Production cross section and current LHC limits for $(gg \rightarrow H \rightarrow h_{125}h_{125}; \text{gray})$, $(gg \rightarrow H \rightarrow WW; \text{red})$, $(gg \rightarrow H \rightarrow ZZ; \text{orange})$ in the $S_{h_{125}}^S - S_{h_{125}}^{NSM}$ plane. *Rows 2–4:* Most relevant branching ratios of H and h_{125} as indicated by the colorbar in the $S_{h_{125}}^S - S_{h_{125}}^{NSM}$ plane for $S_H^S = 0.3$, as in the left panel of the top row. The red stars indicate the benchmark points presented in Table 2. Note that while we do not show the $(h_{125} \rightarrow \tau\tau)$ branching ratio, its scaling with the mixing angles is identical to that of $\text{BR}(h_{125} \rightarrow b\bar{b}; \text{bottom left panel})$, since both of them are down-type fermions.

3 NMSSM Benchmarks

As mentioned earlier, the 2HDM+S is a generalized version of the Next-to-Supersymmetric Standard Model's (NMSSM's) Higgs sector. In Ref. [1] we presented the mapping of both the general and the Z_3 NMSSM to the 2HDM+S. The NMSSM benchmarks presented below are a subset of Z_3 NMSSM benchmarks recently published in Ref. [2]. We reproduce the relevant information here.

In Table 3 we present the NMSSM parameters and mass spectra, in Table 4 the signal strengths, and in Table 5 the most relevant production cross sections and branching ratios for two Benchmark Points, BP1 and BP2. A description of the most important features of the benchmark points can be found below. The benchmark points were chosen as examples of points which are simultaneously within the projected reach of resonant double Higgs search channels with 3000 fb^{-1} and difficult to detect with conventional search strategies.

- BP1: Mono-Higgs
- BP2: Higgs+visible

The benchmark points presented here feature Higgs mass eigenstates approximately aligned with the Higgs basis interaction eigenstates. In particular, they show very small doublet-doublet mixing $|S_{h_{125}}^{\text{NSM}}| < 0.01$ as required by the observed phenomenology of the 125 GeV SM-like state. The doublet-singlet mixing can take somewhat larger values; among the two benchmark points we find the largest mixing angle for BP1 ($S_{h_{125}}^{\text{S}} = 0.117$).

This proximity to the alignment limit is ensured by the values of λ and κ/λ close to what is dictated by the alignment conditions, cf. Refs. [2, 13, 41], and is found to be a generic feature of the allowed NMSSM parameter space we scanned. Note also that for both benchmark points, all non-SM states have masses larger than $m_{h_{125}}/2$. Therefore, h_{125} can only decay into pairs of SM particles. Together with the approximate alignment of h_{125} with H^{SM} , this ensures compatibility of the h_{125} phenomenology with LHC observations.

For both benchmark points, the lighter non SM-like CP-even state h and the lighter CP-odd state a are mostly singlet-like, while the heavier states H and A are dominantly composed of the non SM-like doublet interaction states H^{NSM} and A^{NSM} , respectively.

The mass spectra for the benchmark points are chosen such that the non SM-like doublet-like states H and A are heavy enough to be difficult to detect in conventional searches ($\{m_A, m_H\} \gtrsim 350 \text{ GeV}$) but light enough such that they are readily produced at the LHC. Hence both BP1 and BP2 feature masses of the doublet-like states of $m_A \sim m_H \sim 700 \text{ GeV}$. In order to allow for sufficiently large mass gaps necessary for resonant double Higgs production, the mass of the singlet-like pseudo-scalar states has been chosen considerably lighter than the mass of the doublet-like states, $m_a \sim 200 \text{ GeV}$ for BP1, and $m_a \sim 160 \text{ GeV}$ for BP2. Further, while BP1 features similar singlet masses h and a , BP2 has much larger mass splittings. The corresponding singlet-like scalar masses are $m_h \sim 165 \text{ GeV}$ for BP1, and $m_h \sim 560 \text{ GeV}$ for BP2. Regarding the lightest neutralino, BP1 features $m_{\chi_1} \sim 100 \text{ GeV}$, whereas BP2 features a much heavier neutralino $m_{\chi_1} \sim 500 \text{ GeV}$.

Regarding the branching ratios important for resonant double Higgs production, we first note that the branching ratio of heavy Higgs bosons into pairs of SM-like Higgs bosons

	BP1	BP2
	Mono-Higgs	Higgs+visible
λ	0.602	0.602
κ	-0.281	0.347
$\tan\beta$	2.73	1.40
μ [GeV]	-193	-466
A_λ [GeV]	-784	-270
A_κ [GeV]	-200	26.3
M_A [GeV]	639	732
M_{Q_3} [TeV]	7.66	7.78
$m_{h_{125}}$ [GeV]	127	128
m_h [GeV]	165	561
m_H [GeV]	648	750
m_a [GeV]	205	168
m_A [GeV]	662	749
$(S_{h_{125}}^S)^2$	1.34×10^{-2}	3.96×10^{-3}
$(S_h^S)^2$	0.972	0.986
$(S_H^S)^2$	1.41×10^{-2}	9.78×10^{-3}
$(P_A^S)^2$	5.92×10^{-2}	3.93×10^{-3}
m_{χ_1} [GeV]	102	486
m_{χ_2} [GeV]	212	494
m_{χ_3} [GeV]	292	572

Table 3: NMSSM parameters and mass spectra for our benchmark points. BP1: Mono-Higgs, BP2: Higgs+visible. The first block from the top shows the parameters used as input parameters in `NMSSMTools` $\{\lambda, \kappa, \tan\beta, \mu, A_\lambda, A_\kappa, M_{Q_3}\}$ where the first 6 parameters are those appearing in the scalar potential, and $M_{Q_3} = M_{U_3}$ is the stop mass parameter which controls the radiative corrections to the scalar mass matrices. For the convenience of the reader we also record the value of M_A . The remaining parameters are fixed to $M_1 = M_2 = 1$ TeV, $M_3 = 2$ TeV, $A_t = \mu \cot\beta$, $A_b = \mu \tan\beta$, and all sfermion mass parameters (except $M_{Q_3} = M_{U_3}$) are fixed to 3 TeV. The second block shows the mass spectrum of the Higgs sector, and the third block values of the singlet components of the non SM-like Higgs bosons. In particular, these blocks contain the masses of the CP-odd states a and A and the mixing angle in the CP-odd sector P_A^S . In the fourth block we record the masses of the three lightest neutralinos. Since we set the bino and wino mass parameters to $M_1 = M_2 = 1$ TeV, the two heaviest neutralinos χ_4 and χ_5 are bino- and wino-like with masses $m_{\chi_4} \approx m_{\chi_5} \approx 1$ TeV, while the three lightest neutralinos, χ_1 , χ_2 , and χ_3 , are Higgsino- and singlino-like.

or a SM-like Higgs and a Z boson is suppressed due to the proximity to alignment as

	BP1	BP2
	Mono-Higgs	Higgs+visible V
$\max \left[\mu_{\text{Proj.}}^{300 \text{ fb}^{-1}} (\text{Resonant Higgs production}) \right]$	1.04	0.442
$\max \left[\mu_{\text{Curr. Lim.}}^{<37 \text{ fb}^{-1}} (\text{conventional}) \right]$	8.76×10^{-3}	8.03×10^{-3}
Mono-Higgs Channels		
$\mu_{\text{Proj.}}^{300 \text{ fb}^{-1}} (gg \rightarrow H \rightarrow h_{125} h \rightarrow \gamma\gamma\chi_1\chi_1)$	–	–
$\mu_{\text{Proj.}}^{300 \text{ fb}^{-1}} (gg \rightarrow A \rightarrow h_{125} a \rightarrow \gamma\gamma\chi_1\chi_1)$	1.04	–
Higgs+visible Channels		
$\mu_{\text{Proj.}}^{300 \text{ fb}^{-1}} (gg \rightarrow H \rightarrow h_{125} h \rightarrow b\bar{b}b\bar{b})$	9.93×10^{-2}	5.85×10^{-6}
$\mu_{\text{Proj.}}^{300 \text{ fb}^{-1}} (gg \rightarrow A \rightarrow h_{125} a \rightarrow b\bar{b}b\bar{b})$	2.83×10^{-2}	0.442

Table 4: LHC signal strengths for the benchmark points BP1 and BP2 defined in Table 3. In the first two rows we record the signal strength projected at the LHC for $\mathcal{L} = 300 \text{ fb}^{-1}$ of data in the dominant resonant double Higgs production channel, $\max \left[\mu_{\text{Proj.}}^{300 \text{ fb}^{-1}} (\text{Resonant Higgs production}) \right]$, and the largest signal strength in the conventional channels, $\max \left[\mu_{\text{Curr. Lim.}}^{<37 \text{ fb}^{-1}} (\text{conventional}) \right]$. See Ref. [2] for details. In the remaining rows, we record the projected signal strength at the LHC for $\mathcal{L} = 300 \text{ fb}^{-1}$ of data in the respective final states arising through resonant double Higgs productions.

discussed earlier, see also Refs. [1, 13, 41]. For all benchmark points, we find

$$\begin{aligned} \text{BR}(H \rightarrow h_{125} h_{125}) &\ll \{\text{BR}(H \rightarrow h_{125} h), \text{BR}(A \rightarrow h_{125} a)\}, \\ \text{BR}(A \rightarrow Z h_{125}) &\ll \{\text{BR}(A \rightarrow Zh), \text{BR}(H \rightarrow Za)\}. \end{aligned}$$

Additionally we note that branching ratios of the heavy non-SM like doublets into either h_{125} or Z and an additional singlet like state are generally comparable. This leads to multiple channels that may be probed at the LHC for each benchmark point, as discussed in detail below.

BP1 - Mono-Higgs

This benchmark point features a Higgs spectrum with comparable masses of the singlet-like states a and h , $m_a = 205 \text{ GeV}$ and $m_h = 165 \text{ GeV}$. The heavier states A and H are mostly composed of A^{NSM} and H^{NSM} , respectively, and are approximately mass degenerate with $m_A \approx m_H \approx 650 \text{ GeV}$. The Higgsino mass parameter has a value of $\mu = -193 \text{ GeV}$, and $\kappa = -0.281$, leading to $2|\kappa|/\lambda = 0.93$. Thus, the lightest neutralino χ_1 is mostly singlino-like but has sizable Higgsino components. Its mass is $m_{\chi_1} = 102 \text{ GeV}$, allowing for $(a \rightarrow \chi_1\chi_1)$ decays but not for $(h \rightarrow \chi_1\chi_1)$ decays. The second-lightest neutralino χ_2 is dominantly Higgsino-like with a mass of $m_{\chi_2} = 212 \text{ GeV} \approx |\mu|$, while χ_3 is mostly Higgsino-like but has a sizable singlino component and a mass of $m_{\chi_3} = 292 \text{ GeV}$.

Due to their singlet-like nature, the direct production cross sections of a and h are much smaller than those of a SM Higgs boson of the same mass, rendering them beyond

	BP1	BP2
	Mono-Higgs	Higgs+visible
$\sigma(gg \rightarrow h)$ [pb]	7.10×10^{-2}	1.7×10^{-4}
$\text{BR}(h \rightarrow \tau^+ \tau^-)$	1.74×10^{-2}	3.06×10^{-5}
$\text{BR}(h \rightarrow b\bar{b})$	0.151	2.15×10^{-4}
$\text{BR}(h \rightarrow t\bar{t})$	–	9.34×10^{-4}
$\text{BR}(h \rightarrow \gamma\gamma)$	4.32×10^{-5}	1.31×10^{-6}
$\text{BR}(h \rightarrow ZZ)$	1.77×10^{-2}	6.16×10^{-2}
$\text{BR}(h \rightarrow W^+ W^-)$	0.812	0.128
$\text{BR}(h \rightarrow \chi_1 \chi_1)$	–	–
$\sigma(gg \rightarrow H)$ [pb]	0.134	0.239
$\text{BR}(H \rightarrow \tau^+ \tau^-)$	8.66×10^{-4}	1.82×10^{-4}
$\text{BR}(H \rightarrow b\bar{b})$	6.02×10^{-3}	1.41×10^{-3}
$\text{BR}(H \rightarrow t\bar{t})$	0.281	0.961
$\text{BR}(H \rightarrow \gamma\gamma)$	2.29×10^{-6}	–
$\text{BR}(H \rightarrow ZZ)$	7.31×10^{-5}	6.51×10^{-4}
$\text{BR}(H \rightarrow W^+ W^-)$	1.50×10^{-4}	1.33×10^{-3}
$\text{BR}(H \rightarrow \chi_1 \chi_1)$	6.66×10^{-2}	–
$\text{BR}(H \rightarrow \chi_1 \chi_2)$	0.107	–
$\text{BR}(H \rightarrow \chi_2 \chi_3)$	0.110	–
$\text{BR}(H \rightarrow hh)$	2.46×10^{-3}	–
$\text{BR}(H \rightarrow hh_{125})$	0.102	6.08×10^{-3}
$\text{BR}(H \rightarrow h_{125} h_{125})$	1.73×10^{-3}	8.56×10^{-4}
$\text{BR}(H \rightarrow aa)$	2.47×10^{-3}	1.01×10^{-4}
$\text{BR}(H \rightarrow Za)$	0.308	2.69×10^{-2}
$\sigma(gg \rightarrow a)$ [pb]	0.195	8.36×10^{-2}
$\text{BR}(a \rightarrow \tau^+ \tau^-)$	1.58×10^{-3}	9.05×10^{-2}
$\text{BR}(a \rightarrow b\bar{b})$	1.32×10^{-2}	0.797
$\text{BR}(a \rightarrow \gamma\gamma)$	6.20×10^{-6}	5.60×10^{-3}
$\text{BR}(a \rightarrow \chi_1 \chi_1)$	0.985	–
$\sigma(gg \rightarrow A)$ [pb]	0.175	0.336
$\text{BR}(A \rightarrow \tau^+ \tau^-)$	8.37×10^{-4}	1.60×10^{-4}
$\text{BR}(A \rightarrow b\bar{b})$	5.84×10^{-3}	1.18×10^{-3}
$\text{BR}(A \rightarrow t\bar{t})$	0.350	0.973
$\text{BR}(A \rightarrow \gamma\gamma)$	4.39×10^{-6}	7.95×10^{-6}
$\text{BR}(A \rightarrow \chi_1 \chi_1)$	0.102	–
$\text{BR}(A \rightarrow \chi_3 \chi_3)$	0.112	–
$\text{BR}(A \rightarrow ha)$	3.31×10^{-3}	2.69×10^{-4}
$\text{BR}(A \rightarrow h_{125} a)$	0.304	1.88×10^{-2}
$\text{BR}(A \rightarrow Zh)$	8.40×10^{-2}	4.00×10^{-3}
$\text{BR}(A \rightarrow Zh_{125})$	5.61×10^{-4}	2.86×10^{-4}

Table 5: Gluon fusion production cross sections at the $\sqrt{s} = 13$ TeV LHC, $\sigma(gg \rightarrow \Phi)$, as well as the most relevant branching ratios for the non SM-like Higgs bosons $\Phi = \{h, H, a, A\}$ for the benchmark points BP1 and BP4 defined in Table 3.

the reach of conventional search channels at the LHC which rely on direct production of a or h . The dominant decay modes of h are into pairs of b -quarks, and, facilitated by its (small) doublet component, into pairs of W -bosons. The singlet-like pseudo-scalar on the other hand is kinematically allowed to decay into pairs of neutralinos ($a \rightarrow \chi_1 \chi_1$). Because χ_1 has sizable singlino as well as Higgsino components, such decays proceed via both of the NMSSM's large couplings λ and κ , rendering the corresponding branching ratio large, $\text{BR}(a \rightarrow \chi_1 \chi_1) = 0.985$.

The heavier (doublet-like) CP-even state H mostly decays into pairs of top quarks, neutralinos, and, most relevant for resonant double Higgs production, via ($H \rightarrow hh_{125}$) and ($H \rightarrow Za$). The cross section ($gg \rightarrow H \rightarrow hh_{125}$) is not large enough for it to be within reach of the Higgs+visible search modes. However, facilitated by the sizable branching ratios of ($H \rightarrow Za$) and ($a \rightarrow \chi_1 \chi_1$), this benchmark point is within the projected reach of mono- Z searches, $\mu_{\text{Proj.}}^{3000 \text{ fb}^{-1}}(gg \rightarrow H \rightarrow Za \rightarrow \ell^+ \ell^- \chi_1 \chi_1) = 1.73$ at the LHC with 3000 fb^{-1} of data [2].

The heavier (doublet-like) CP-odd state A mostly decays into pairs of top quarks, neutralinos, and through the ($A \rightarrow h_{125}a$) channel. The sizable branching ratio of the latter decay mode, $\text{BR}(A \rightarrow Zh_{125}) = 0.304$, together with the large branching ratio corresponding to ($a \rightarrow \chi_1 \chi_1$) decays leads to a large projected signal strength in mono-Higgs searches via the corresponding decay chain, $\mu_{\text{Proj.}}^{300 \text{ fb}^{-1}}(gg \rightarrow A \rightarrow h_{125}a \rightarrow \gamma\gamma\chi_1\chi_1) = 1.04$.

Neither H nor A have large branching ratios into pairs of SM states except into pairs of top quarks, rendering them very difficult to detect by conventional searches.

BP2 - Higgs+visible

Benchmark point BP2 features a Higgs spectrum with a large split between the masses of the singlet-like states a and h , $m_a = 168 \text{ GeV}$ and $m_h = 561 \text{ GeV}$. The heavier doublet-like states A and H are almost mass degenerate, $m_A \approx m_H \approx 750 \text{ GeV}$. The Higgsino mass parameter takes much larger absolute value than for BP1, $\mu = -466 \text{ GeV}$. Further, κ also has a larger absolute value than for BP1, $\kappa = 0.347$, leading to $2|\kappa|/\lambda = 1.15$. Thus, the two lightest neutralinos, χ_1 and χ_2 , are mostly Higgsino like and approximately mass degenerate, $m_{\chi_1} = 486 \text{ GeV}$ and $m_{\chi_2} = 494 \text{ GeV}$. The third-lightest neutralino, χ_3 , is mostly composed of the singlino and has a mass of $m_{\chi_3} = 572 \text{ GeV}$. Note that because $|2|\kappa|/\lambda - 1|$ is larger than for BP1, the Higgsino and singlino mass parameters are split further for BP2 than for BP1, leading to much smaller singlino-Higgsino mixing. Further, because of the relatively large masses of the neutralinos, none of the Higgs bosons are kinematically allowed to decay into pairs of neutralinos.

Similar to BP1, the large singlet components of a and h lead to direct production cross sections at the LHC much smaller than those of SM Higgs bosons of the same mass. Thus, they are out of reach of conventional search strategies. The dominant decay mode of the CP-even state h is into pairs of W -bosons and pairs of the much lighter singlet-like CP-odd state, $\text{BR}(h \rightarrow aa) = 0.740$. The CP-odd state a decays mostly into pairs of b -quarks with a branching ratio of $\text{BR}(a \rightarrow b\bar{b}) = 0.797$. It also has a sizable branching ratio into τ -leptons, $\text{BR}(a \rightarrow \tau^+ \tau^-) = 0.0905$.

The heavier (doublet-like) CP-even state H predominantly decays into pairs of top quarks. Because of the small value of $\tan\beta$ compared to BP1, $(H \rightarrow h_{125}h)$ decays, which are mostly controlled by the $(H^{\text{SM}}H^{\text{NSM}}H^{\text{S}})$ coupling, are suppressed. The largest branching ratio of H relevant for non standard Higgs decays is $\text{BR}(H \rightarrow Za) = 0.0269$. However, this branching ratio is not sufficiently large to put BP2 within reach of Z +visible searches where the projected signal strength with 3000 fb^{-1} of data is only $\mu_{\text{Proj.}}^{3000 \text{ fb}^{-1}}(gg \rightarrow H \rightarrow Za \rightarrow \ell^+\ell^-\chi_1\chi_1) = 0.136$ [2].

Similar to H , the CP-odd doublet-like state A mostly decays into pairs of top quarks. The largest branching ratio relevant for resonant double Higgs production is $\text{BR}(A \rightarrow h_{125}a) = 0.0188$. This decay mode is mostly controlled by the $(H^{\text{SM}}A^{\text{NSM}}A^{\text{S}})$ coupling, which becomes largest for values of $\tan\beta = 1$, but is suppressed for $\text{sgn}(\kappa) = +1$. Nonetheless, together with the large branching ratio of a into pairs of b -quarks, this branching ratio is sufficiently large to render BP2 within reach of Higgs+visible searches with a projected signal strength $\mu_{\text{Proj.}}^{3000 \text{ fb}^{-1}}(gg \rightarrow A \rightarrow h_{125}a \rightarrow b\bar{b}b\bar{b}) = 1.22$ with 3000 fb^{-1} of data. With 300 fb^{-1} of data, the projected signal strength is $\mu_{\text{Proj.}}^{300 \text{ fb}^{-1}}(gg \rightarrow A \rightarrow h_{125}a \rightarrow b\bar{b}b\bar{b}) = 0.442$.

Since both H and A decay dominantly into pairs of top quarks, BP2 is very challenging to discover with conventional search strategies.

4 Conclusions

The 2HDM+S provides a well motivated framework for analyzing the complex phenomenology which may result from more complete models such as the NMSSM. The mapping from both the general and the Z_3 NMSSM to the 2HDM+S parameters is given in Ref. [1].

We have presented benchmark scenarios in the 2HDM+S optimized for three sets of signatures which may be probed with 300 fb^{-1} of data at the LHC:

- $A \rightarrow h_{125}a$, $H \rightarrow h_{125}h$,
- $A \rightarrow ah$, $H \rightarrow hh$, $H \rightarrow aa$, and
- $H \rightarrow h_{125}h_{125}$.

We have also presented benchmark points in the NMSSM previously published in Ref. [2], which while being optimized for $(A \rightarrow h_{125}a, H \rightarrow h_{125}h)$ show the complementarity of the different possible channels, in particular decays involving a Z boson in the final state.

Acknowledgments

We thank the conveners of the LHCHSWG-HH working group for encouraging our work on this note. We also thank the members of the working group for useful discussions which lead to the present form of the note. SB acknowledges support by the Vetenskapsrådet (Swedish Research Council) through contract No. 638-2013-8993 and the Oskar Klein Centre for Cosmoparticle Physics. NRS is supported by DoE grant DE-SC0007983 and Wayne State University.

References

- [1] S. Baum and N. R. Shah, *Two Higgs Doublets and a Complex Singlet: Disentangling the Decay Topologies and Associated Phenomenology*, *JHEP* **12** (2018) 044, [[1808.02667](#)].
- [2] S. Baum, N. R. Shah and K. Freese, *The NMSSM is within Reach of the LHC: Mass Correlations & Decay Signatures*, *JHEP* **04** (2019) 011, [[1901.02332](#)].
- [3] K. S. Babu and S. Jana, *Enhanced Di-Higgs Production in the Two Higgs Doublet Model*, *JHEP* **02** (2019) 193, [[1812.11943](#)].
- [4] A. Adhikary, S. Banerjee, R. Kumar Barman and B. Bhattacharjee, *Resonant heavy Higgs searches at the HL-LHC*, [1812.05640](#).
- [5] P. Basler, S. Dawson, C. Englert and M. Mühlleitner, *Showcasing HH production: Benchmarks for the LHC and HL-LHC*, *Phys. Rev.* **D99** (2019) 055048, [[1812.03542](#)].
- [6] H. Georgi and D. V. Nanopoulos, *Suppression of Flavor Changing Effects From Neutral Spinless Meson Exchange in Gauge Theories*, *Phys. Lett.* **B82** (1979) 95–96.
- [7] J. F. Donoghue and L. F. Li, *Properties of Charged Higgs Bosons*, *Phys. Rev.* **D19** (1979) 945.
- [8] J. Gunion, H. Haber, G. Kane and S. Dawson, *The Higgs Hunter’s Guide*. Frontiers in Physics. Westview Press, 2008.
- [9] L. Lavoura and J. P. Silva, *Fundamental CP violating quantities in a $SU(2) \times U(1)$ model with many Higgs doublets*, *Phys. Rev.* **D50** (1994) 4619–4624, [[hep-ph/9404276](#)].
- [10] F. J. Botella and J. P. Silva, *Jarlskog - like invariants for theories with scalars and fermions*, *Phys. Rev.* **D51** (1995) 3870–3875, [[hep-ph/9411288](#)].
- [11] G. C. Branco, L. Lavoura and S. J.P., *CP violation*. Oxford University Press, Oxford, UK, 1999.
- [12] J. F. Gunion and H. E. Haber, *The CP conserving two Higgs doublet model: The Approach to the decoupling limit*, *Phys. Rev.* **D67** (2003) 075019, [[hep-ph/0207010](#)].
- [13] M. Carena, H. E. Haber, I. Low, N. R. Shah and C. E. M. Wagner, *Alignment limit of the NMSSM Higgs sector*, *Phys. Rev.* **D93** (2016) 035013, [[1510.09137](#)].
- [14] LHC HIGGS CROSS SECTION WORKING GROUP collaboration, D. de Florian et al., *Handbook of LHC Higgs Cross Sections: 4. Deciphering the Nature of the Higgs Sector*, [1610.07922](#).
- [15] R. V. Harlander, S. Liebler and H. Mantler, *SusHi: A program for the calculation of Higgs production in gluon fusion and bottom-quark annihilation in the Standard Model and the MSSM*, *Comput. Phys. Commun.* **184** (2013) 1605–1617, [[1212.3249](#)].
- [16] R. V. Harlander, S. Liebler and H. Mantler, *SusHi Bento: Beyond NNLO and the heavy-top limit*, *Comput. Phys. Commun.* **212** (2017) 239–257, [[1605.03190](#)].
- [17] S. Liebler, *Neutral Higgs production at proton colliders in the CP-conserving NMSSM*, *Eur. Phys. J.* **C75** (2015) 210, [[1502.07972](#)].
- [18] R. V. Harlander and W. B. Kilgore, *Next-to-next-to-leading order Higgs production at hadron colliders*, *Phys. Rev. Lett.* **88** (2002) 201801, [[hep-ph/0201206](#)].
- [19] U. Aglietti, R. Bonciani, G. Degrossi and A. Vicini, *Two loop light fermion contribution to Higgs production and decays*, *Phys. Lett.* **B595** (2004) 432–441, [[hep-ph/0404071](#)].

- [20] R. Bonciani, G. Degrossi and A. Vicini, *On the Generalized Harmonic Polylogarithms of One Complex Variable*, *Comput. Phys. Commun.* **182** (2011) 1253–1264, [[1007.1891](#)].
- [21] G. Degrossi and P. Slavich, *NLO QCD bottom corrections to Higgs boson production in the MSSM*, *JHEP* **11** (2010) 044, [[1007.3465](#)].
- [22] G. Degrossi, S. Di Vita and P. Slavich, *NLO QCD corrections to pseudoscalar Higgs production in the MSSM*, *JHEP* **08** (2011) 128, [[1107.0914](#)].
- [23] G. Degrossi, S. Di Vita and P. Slavich, *On the NLO QCD Corrections to the Production of the Heaviest Neutral Higgs Scalar in the MSSM*, *Eur. Phys. J.* **C72** (2012) 2032, [[1204.1016](#)].
- [24] R. Harlander and P. Kant, *Higgs production and decay: Analytic results at next-to-leading order QCD*, *JHEP* **12** (2005) 015, [[hep-ph/0509189](#)].
- [25] K. G. Chetyrkin, J. H. Kuhn and M. Steinhauser, *RunDec: A Mathematica package for running and decoupling of the strong coupling and quark masses*, *Comput. Phys. Commun.* **133** (2000) 43–65, [[hep-ph/0004189](#)].
- [26] <http://www.th.u-psud.fr/NMHDECAY/nmssmtools.html>.
- [27] U. Ellwanger, J. F. Gunion and C. Hugonie, *NMHDECAY: A Fortran code for the Higgs masses, couplings and decay widths in the NMSSM*, *JHEP* **02** (2005) 066, [[hep-ph/0406215](#)].
- [28] U. Ellwanger and C. Hugonie, *NMHDECAY 2.0: An Updated program for sparticle masses, Higgs masses, couplings and decay widths in the NMSSM*, *Comput. Phys. Commun.* **175** (2006) 290–303, [[hep-ph/0508022](#)].
- [29] D. Das, U. Ellwanger and A. M. Teixeira, *NMSDECAY: A Fortran Code for Supersymmetric Particle Decays in the Next-to-Minimal Supersymmetric Standard Model*, *Comput. Phys. Commun.* **183** (2012) 774–779, [[1106.5633](#)].
- [30] M. Mühlleitner, A. Djouadi and Y. Mambrini, *SDECAY: A Fortran code for the decays of the supersymmetric particles in the MSSM*, *Comput. Phys. Commun.* **168** (2005) 46–70, [[hep-ph/0311167](#)].
- [31] S. Baum, M. Carena, N. R. Shah and C. E. M. Wagner, *Higgs portals for thermal Dark Matter. EFT perspectives and the NMSSM*, *JHEP* **04** (2018) 069, [[1712.09873](#)].
- [32] D. Dicus, A. Stange and S. Willenbrock, *Higgs decay to top quarks at hadron colliders*, *Phys. Lett.* **B333** (1994) 126–131, [[hep-ph/9404359](#)].
- [33] R. Barcelo and M. Masip, *Extra Higgs bosons in $t\bar{t}$ production at the LHC*, *Phys. Rev.* **D81** (2010) 075019, [[1001.5456](#)].
- [34] V. Barger, W.-Y. Keung and B. Yencho, *Azimuthal Correlations in Top Pair Decays and The Effects of New Heavy Scalars*, *Phys. Rev.* **D85** (2012) 034016, [[1112.5173](#)].
- [35] Y. Bai and W.-Y. Keung, *Can vanishing mass-on-shell interactions generate a dip at colliders?*, *Int. J. Mod. Phys.* **A30** (2015) 1550120, [[1407.6355](#)].
- [36] S. Jung, J. Song and Y. W. Yoon, *Dip or nothingness of a Higgs resonance from the interference with a complex phase*, *Phys. Rev.* **D92** (2015) 055009, [[1505.00291](#)].
- [37] N. Craig, F. D’Eramo, P. Draper, S. Thomas and H. Zhang, *The Hunt for the Rest of the Higgs Bosons*, *JHEP* **06** (2015) 137, [[1504.04630](#)].
- [38] S. Gori, I.-W. Kim, N. R. Shah and K. M. Zurek, *Closing the Wedge: Search Strategies for Extended Higgs Sectors with Heavy Flavor Final States*, *Phys. Rev.* **D93** (2016) 075038, [[1602.02782](#)].

- [39] M. Carena and Z. Liu, *Challenges and opportunities for heavy scalar searches in the $t\bar{t}$ channel at the LHC*, *JHEP* **11** (2016) 159, [[1608.07282](#)].
- [40] U. Ellwanger and M. Rodriguez-Vazquez, *Simultaneous search for extra light and heavy Higgs bosons via cascade decays*, *JHEP* **11** (2017) 008, [[1707.08522](#)].
- [41] S. Baum, K. Freese, N. R. Shah and B. Shakya, *NMSSM Higgs boson search strategies at the LHC and the mono-Higgs signature in particular*, *Phys. Rev.* **D95** (2017) 115036, [[1703.07800](#)].
- [42] ATLAS collaboration, *Search for pair production of Higgs bosons in the $b\bar{b}b\bar{b}$ final state using proton-proton collisions at $\sqrt{s} = 13$ TeV with the ATLAS detector*, Tech. Rep. ATLAS-CONF-2016-017, CERN, Geneva, Mar, 2016.
- [43] CMS collaboration, *Search for resonant pair production of Higgs bosons decaying to two bottom quark-antiquark pairs in proton-proton collisions at 13 TeV*, Tech. Rep. CMS-PAS-HIG-16-002, CERN, Geneva, 2016.
- [44] ATLAS collaboration, *Search for pair production of Higgs bosons in the $b\bar{b}b\bar{b}$ final state using proton-proton collisions at $\sqrt{s} = 13$ TeV with the ATLAS detector*, Tech. Rep. ATLAS-CONF-2016-049, CERN, Geneva, Aug, 2016.
- [45] CMS collaboration, *Search for resonant pair production of Higgs bosons decaying to bottom quark-antiquark pairs in proton-proton collisions at 13 TeV*, Tech. Rep. CMS-PAS-HIG-17-009, CERN, Geneva, 2017.
- [46] CMS collaboration, *Search for $H(bb)H(\text{gammagamma})$ decays at 13TeV*, Tech. Rep. CMS-PAS-HIG-16-032, CERN, Geneva, 2016.
- [47] ATLAS collaboration, *Search for Higgs boson pair production in the $b\bar{b}\gamma\gamma$ final state using pp collision data at $\sqrt{s} = 13$ TeV with the ATLAS detector*, Tech. Rep. ATLAS-CONF-2016-004, CERN, Geneva, Mar, 2016.
- [48] CMS collaboration, *Search for Higgs boson pair production in the final state containing two photons and two bottom quarks in proton-proton collisions at $\sqrt{s} = 13$ TeV*, Tech. Rep. CMS-PAS-HIG-17-008, CERN, Geneva, 2017.
- [49] ATLAS, CMS collaboration, G. Aad et al., *Measurements of the Higgs boson production and decay rates and constraints on its couplings from a combined ATLAS and CMS analysis of the LHC pp collision data at $\sqrt{s} = 7$ and 8 TeV*, *JHEP* **08** (2016) 045, [[1606.02266](#)].
- [50] CMS collaboration, A. M. Sirunyan et al., *Measurements of properties of the Higgs boson decaying into the four-lepton final state in pp collisions at $\sqrt{s} = 13$ TeV*, *JHEP* **11** (2017) 047, [[1706.09936](#)].
- [51] CMS collaboration, A. M. Sirunyan et al., *Measurements of properties of the Higgs boson decaying to a W boson pair in pp collisions at $\sqrt{s} = 13$ TeV*, *Phys. Lett.* **B791** (2019) 96, [[1806.05246](#)].
- [52] CMS collaboration, A. M. Sirunyan et al., *Combined measurements of Higgs boson couplings in proton-proton collisions at $\sqrt{s} = 13$ TeV*, Submitted to: *Eur. Phys. J.* (2018) , [[1809.10733](#)].
- [53] ATLAS collaboration, *Combined measurements of Higgs boson production and decay in the $H \rightarrow ZZ \rightarrow 4\ell$ and $H \rightarrow \gamma\gamma$ channels using $\sqrt{s} = 13$ TeV pp collision data collected with the ATLAS experiment*, Tech. Rep. ATLAS-CONF-2017-047, CERN, Geneva, Jul, 2017.

- [54] *Search for diboson resonances in the $\ell\ell qq$ final state in pp collisions at $\sqrt{s} = 13$ TeV with the ATLAS detector*, Tech. Rep. ATLAS-CONF-2015-071, CERN, Geneva, Dec, 2015.
- [55] *Search for high-mass resonances decaying into a Z boson pair in the $\ell\ell\nu\nu$ final state in pp collisions at $\sqrt{s} = 13$ TeV with the ATLAS detector*, Tech. Rep. ATLAS-CONF-2016-012, CERN, Geneva, Mar, 2016.
- [56] *Search for ZZ resonances in the $\ell\ell qq$ final state in pp collisions at $\sqrt{s} = 13$ TeV with the ATLAS detector*, Tech. Rep. ATLAS-CONF-2016-016, CERN, Geneva, Mar, 2016.
- [57] CMS COLLABORATION collaboration, *Search for a heavy scalar boson decaying into a pair of Z bosons in the $2\ell 2\nu$ final state*, Tech. Rep. CMS-PAS-HIG-16-001, CERN, Geneva, 2016.
- [58] CMS COLLABORATION collaboration, *Measurements of properties of the Higgs boson and search for an additional resonance in the four-lepton final state at $\sqrt{s} = 13$ TeV*, Tech. Rep. CMS-PAS-HIG-16-033, CERN, Geneva, 2016.
- [59] ATLAS COLLABORATION collaboration, *Search for new phenomena in the $Z(\rightarrow \ell\ell) + E_{\text{T}}^{\text{miss}}$ final state at $\sqrt{s} = 13$ TeV with the ATLAS detector*, Tech. Rep. ATLAS-CONF-2016-056, CERN, Geneva, Aug, 2016.
- [60] ATLAS COLLABORATION collaboration, *Study of the Higgs boson properties and search for high-mass scalar resonances in the $H \rightarrow ZZ^* \rightarrow 4\ell$ decay channel at $\sqrt{s} = 13$ TeV with the ATLAS detector*, Tech. Rep. ATLAS-CONF-2016-079, CERN, Geneva, Aug, 2016.
- [61] ATLAS collaboration, M. Aaboud et al., *Search for heavy ZZ resonances in the $\ell^+\ell^-\ell^+\ell^-$ and $\ell^+\ell^-\nu\bar{\nu}$ final states using proton-proton collisions at $\sqrt{s} = 13$ TeV with the ATLAS detector*, *Eur. Phys. J.* **C78** (2018) 293, [[1712.06386](#)].
- [62] CMS collaboration, A. M. Sirunyan et al., *Search for a new scalar resonance decaying to a pair of Z bosons in proton-proton collisions at $\sqrt{s} = 13$ TeV*, *JHEP* **06** (2018) 127, [[1804.01939](#)].
- [63] ATLAS collaboration, *Search for a high-mass Higgs boson decaying to a pair of W bosons in pp collisions at $\sqrt{s}=13$ TeV with the ATLAS detector*, Tech. Rep. ATLAS-CONF-2016-021, CERN, Geneva, Apr, 2016.
- [64] CMS collaboration, *Search for high mass Higgs to WW with fully leptonic decays using 2015 data*, Tech. Rep. CMS-PAS-HIG-16-023, CERN, Geneva, 2016.
- [65] ATLAS collaboration, *Search for a high-mass Higgs boson decaying to a pair of W bosons in pp collisions at $\sqrt{s}=13$ TeV with the ATLAS detector*, Tech. Rep. ATLAS-CONF-2016-074, CERN, Geneva, Aug, 2016.
- [66] ATLAS collaboration, *Search for diboson resonance production in the $\ell\nu qq$ final state using pp collisions at $\sqrt{s} = 13$ TeV with the ATLAS detector at the LHC*, Tech. Rep. ATLAS-CONF-2016-062, CERN, Geneva, Aug, 2016.
- [67] ATLAS collaboration, M. Aaboud et al., *Search for heavy resonances decaying into WW in the $e\nu\mu\nu$ final state in pp collisions at $\sqrt{s} = 13$ TeV with the ATLAS detector*, *Eur. Phys. J.* **C78** (2018) 24, [[1710.01123](#)].
- [68] ATLAS collaboration, M. Aaboud et al., *Search for WW/WZ resonance production in $\ell\nu qq$ final states in pp collisions at $\sqrt{s} = 13$ TeV with the ATLAS detector*, [[1710.07235](#)].
- [69] CMS COLLABORATION collaboration, *Search for a heavy Higgs boson decaying to a pair of W bosons in proton-proton collisions at $\sqrt{s} = 13$ TeV*, Tech. Rep. CMS-PAS-HIG-17-033, CERN, Geneva, 2019.